UNIVERSITY OF HELSINKI REPORT SERIES IN PHYSICS

HU-P-D222

Structural modification of graphene by ion irradiation studied with molecular dynamics simulations

Elina Harriet Åhlgren

Division of Materials Physics
Department of Physics
Faculty of Science
University of Helsinki
Helsinki, Finland

ACADEMIC DISSERTATION

To be presented, with the permission of the Faculty of Science of the University of Helsinki, for public criticism in auditorium A110 of the Department of Chemistry (Chemicum), on 12th December 2014 at 12 o'clock p.m.

HELSINKI 2014

ISBN 978-952-10-8971-8 (printed version)
ISSN 0356-0961
Helsinki 2014
Unigrafia
ISBN 978-952-10-8972-5 (PDF version)
http://ethesis.helsinki.fi/
Helsinki 2014
Electronic Publications @ University of Helsinki

Science.

What is that? A collection of complicated formulas one had to learn in school to pass the physics course? No, there has to be more to it. A way of seeing the world, understanding the laws governing it. The sort of thing that hides in the mountains which rise up to the smokey clouds implying things only the sort of mountains can imply. Great things. Scientists peer up the rocky walls trying to catch a glimpse of something nobody has seen before. They formulate hypotheses and try out theories for the greater good of knowledge and possibly even humanity. Spending countless hours in dusty laboratories with computers and humming gadgets. Sometimes, they will even find something new. Scientists are a breed of their own. Always searching, testing, questioning even the simplest truths and throwing away old beliefs every time those are proven wrong. The sort of dedication this needs can only arise out of pure love for what they do. Who else would even start to question the nature of matter? A particle is a particle, right, not a wave, is it? This breed has taken up a quest of knowledge and of understanding the world around us. With this humble effort in the form of this thesis, I am taking a step closer to join the scientists with their quest. I am uncertain if I am truly up to the task, but in science not knowing is the essential part of the fun.

Elina Harriet Åhlgren, **Structural modification of graphene by ion irradiation studied with molecular dynamics simulations**, University of Helsinki, 2014, 55 p. + appendices, University of Helsinki Report Series in Physics HU-P-D222, ISSN 0356-0961, ISBN 978-952-10-8971-8 (printed version), ISBN 978-952-10-8972-5 (PDF version)

Abstract

Graphene is a two-dimensional one-atomic-layer-thick material, which existence was predicted theoretically already in the 40's. Only in 2004 the first reported samples were obtained. After that, the properties of graphene have proved to be extreme in many ways. To name a few, it is one of the mechanically strongest materials known, one square meter of it weights less than one milligram, it prevents even the smallest gas particles from penetrating it and it has very high electronic conductivity.

For a material to be suitable for specific applications in industry, the intrinsic form of it does not always cut for what is demanded by the application. One should be able to modify the structure and the properties of the material to fit the purpose in hand. Because graphene is a 2D material, the used method has to be precise enough to tune the structure one atom at a time. Irradiation with energetic particles fits this purpose and it has been used by the industry for e.g. shaping bulk materials to create thin films. The novelty is, that it has not been used in such a precision as demanded by nanoscale materials. Studying the irradiation response of graphene provides further understanding of the prospects of this material for device applications.

This thesis discusses modification of graphene via energetic particle bombardment in detail. Taking different aspects provides a vast understanding of the dynamics of defect production in graphene. The studied systems vary from freestanding graphene to metal supported membrane. The effect of the irradiation changes by the type and energy of the ion. Atomistic simulations provide the needed theoretical tool for modeling the atomic scale behavior of the system during the irradiation process. This type of detailed information on the system dynamics would be impossible to achieve with existing experimental tools. Parts of the presented work is done in collaboration with experimental groups. These collaborations are an important part of the studies as the simulations aim to provide information on real systems.

By choosing the right energy for the bombarding ion, the defect types can be predicted and chosen to fit the purpose of the experiment. At the low energy regime up to hundreds of keV's, the interaction between the ion and the lattice atoms is controlled by the ionic collisions. This suggests that the produced defects are small, consisting of only few atoms that take part in the actual atomic collision.

Choosing a low irradiation energy and an ion comparable to the lattice atoms in size, namely boron or nitrogen in the case of graphene, the ion could in principle be stopped at the membrane and even be used to substitute a lattice atom. This is called doping, and it affects the electronic properties of the material. The presented results indicate that the doping of graphene is possible with ion beams and the highest probability for a carbon atom to be replaced by boron or nitrogen is at the energy of about 50 eV. Other defect types such as single vacancies and dopant atoms have separate energy ranges where they are the most likely configurations after irradiation. Therefore, by choosing the ion and the energy carefully, they can be either avoided or used for extremely precise patterning of graphene.

For continuous irradiation, a simple model is constructed to evaluate the amount of atoms leaving the target and to predict the amount of defects graphene can withstand. The calculations show that even with high vacancy concentrations up to 35%, the graphene membrane remains stable. As the graphene sheet is placed on top of a metal substrate, the irradiation response changes. At energies below 1 keV, the defect production decreases compared to the freestanding membrane as the substrate stopsthe carbon atoms from escaping. At higher energies the effect is the opposite, the ion can penetrate the graphene sheet and scatter atoms from the metal surface. These atoms can then bombard the overlying graphene from below creating more defects in the membrane.

What becomes of the atoms that are stuck at the area between the graphene and the metal? According to the simulations, there can be more than two carbon atoms trapped for each incoming ion. The amount is substantial, and a new quantity called trapping yield is introduced. It describes the irradiation features of supported graphene. In the experiments, upon annealing, these trapped atoms start to form small graphene platelets at the interface under the continuous graphene network, creating new nanostructures observed with scanning tunneling microscopy.

With high bombarding energies in the range of MeV's, the defect production mechanism differs from the lower energy range. The impacts of the ion's electrons with the target are the main interaction mechanism, and the actual impact of the ion itself is not as important. The inelastic scattering of electrons increases the thermal energy of the lattice locally at the path of the ion. The defects created in the freestanding membrane are hole-like. The diameter of the holes changes from few nm's up to tens of nm's and can be varied with the type and energy of the ion.

The presented simulations provide data on precise patterning of graphene, which can be of great use when planning structural modification of this nanoscaled material using ion beams. The carefully selected irradiation parameters are in the central part of controlling the type of the created damage. The precisions changes from single atoms to tens of nm's, giving multiple options for patterning graphene.

Contents

Chapter 1

Introduction

Material research is characterized by testing and measuring the properties of different types of materials, finding properties fit for specific applications, and molding them to fit the purpose at hand even better. Not too long ago, we had a rather limited amount of tools in the toolbox, as the range of known materials was relatively restricted. What started by stone, water, fire and air, developed during the centuries and nowadays the eras of early human civilization are named by the tools that were in the center of those times, The Stone Age, The Bronze Age and the Iron Age. Over the past 100 years, scientists have learned to understand the physics of materials, how the atomic and electronic structure affects the properties, and gives the material its specific features. This knowledge opened a door to shape and tune the characteristics of materials to satisfy the requirements of the society, creating numerous new materials along the way and leading to the Modern Era.

As it comes to novel materials, in the 21st century science has provided new materials, scaling down to the nanometer-size in one or multiple dimensions, in order to satisfy the growing needs of industry, such as smaller and faster electronics. These atomic scale materials have different properties compared to the traditional three-dimensional materials. They are light and small, offering new prospects in the scale of device manufacturing. Some of them have other promising features such as high electrical conductivity or magnetism. Graphene is a material with a two-dimensional lattice, as it spreads in two dimensions but in the third dimension, along the z-axis, it is only one atomic layer thick . Although its existence was predicted as a theoretical model already in the 1940's [1], one layer thick graphene is still fairly new to the game produced successfully only in 2004 [2]. Graphene has the potential to be the building block for next-generation electronics, but there is a gap that has to be crossed, or more precisely, a gap that has to be created. Pristine graphene is a semimetal with no band gap as the valence and conduction bands in the electronic structure are touching. This allows electrons to move freely. In the eyes of electronic applications, this is not desirable. With a gap, the conductance of the device can be controlled, as the electrons can be excited over it with a certain amount of energy. By

introducing defects into the lattice, a gap can be opened [3]. How to tune the atomic lattice to fit the requirements of an application is still not completely clear, and further understanding of the defect production mechanisms is needed.

The aim of this thesis is to study the subject of how the lattice structure of graphene can be altered in a controlled manner, using ion irradiation to tailor the properties of the material. Collaborations with international experimental groups enables direct comparison between experiments and simulation results, offering a broad view of the subject. In publications **I-II** low energy ion irradiation response of freestanding graphene is studied using molecular dynamics simulations, while publications **III-IV** concentrate on the low energy ion irradiation of graphene grown on a metal substrate. The studies compare experimental results from scanning tunneling microscopy and atomistic simulations. Publication **V** focuses on the features of swift heavy ion irradiation of graphene, providing the first work at the high energy spectrum of the irradiation. In the publication two temperature molecular dynamics is applied to model the defect production in graphene via an inelastic thermal spike model.

Chapter 2

Purpose and structure of this study

This thesis provides detailed informations on controllable ways to modify the atomic structure of graphene using ion irradiation. The irradiation response of freestanding and supported graphene is studied using analytical potentials and molecular dynamics simulations complementary to collaborations with experimental researchers. In particular, ion irradiation is used to modify the atomic structure of graphene atom by atom, in order to learn the specific defect production mechanisms that cannot be observed in the experiments. The obtained results indicate the appropriate choices of ion species and energies to achieve a specific type of lattice modification. The energy of the chosen ion has a significant impact on the type of the defect it produces. As graphene is often grown on a substrate, this is also addressed in the study and detailed analysis on the irradiation features of freestanding and metal supported graphene is given.

This thesis consists of a summary and five research articles which have been either published (3), submitted for publication (1) or in preparation (1) for international peer-reviewed journals. Within the text, the articles are referred by bold face Roman numerals and they are included at the end of the thesis.

The structure of the summary is presented in the following. In this chapter, the publications are shortly discussed, as well as the author's contributions to each paper. In chapter three the studied material, graphene, is presented starting from the history of the material, shortly reviewing the synthesizing methods, and proceeding to the most important mechanical and electronic properties. In chapter four, the used methods are discussed starting with ion irradiation and continuing with a description of the simulation methods and the experimental method used by the collaborators. Chapter five concentrates on the atomic scale engineering of graphene as presented in the publications, including analysis of low and high energy irradiation of freestanding as well as metal supported graphene with various energies and ions. Finally, the conclusions are given in chapter six.

2.1 Summaries of the original publications

Publication I: Atomistic simulations of the implantation of low-energy boron and nitrogen ions into graphene,
E. H. Åhlgren, J. Kotakoski, and A. V. Krasheninnikov, *Physical Review B* **83**, 115424 (2011).

This work is dedicated to understanding the mechanisms of doping of graphene with boron and nitrogen ions. These two ion species are the natural dopants of graphene, and provide a path for tuning the material's electronic properties, introducing more electrons into the lattice or subsequently reducing them. The irradiation response is studied as a function of the ion energy for both of the dopants. The results obtained from molecular dynamics simulations indicate clearly separate energies for different defect configurations including the substitutional site, providing information for experimental doping of graphene.

Publication II: Ion irradiation tolerance of graphene as studied by atomistic simulations,
E. H. Åhlgren, J. Kotakoski, O. Lehtinen, and A. V. Krasheninnikov, *Applied Physics Letters* **100**, 233108 (2012).

This publication focuses on the accumulation of irradiation-induced damage in graphene membranes via atomistic simulations. The results show that even with high vacancy concentrations, studied up to 35%, the membrane shows no signs of mechanical failure. This provides support for the use of graphene membranes as a window material for separating vacuum from ambient conditions in ion beam systems. The results produce estimates for the sputtering yield of graphene that can be applied during experiments, in order to estimate the amount of created damage.

Publication III: Structural manipulation of the graphene/metal interface with Ar^+ irradiation,

E. H. Åhlgren, S. K. Hämäläinen, O. Lehtinen, P. Liljeroth, and J. Kotakoski, *Physical Review B* **88**, 155419 (2013).

Graphene is often grown on a metal substrate for large scale manufacturing of the material. However, when modification of the atomic structure is done by ion irradiation,

the irradiation response changes, depending on whether the membrane is freestanding or supported. In this paper, the defect production in supported graphene is studied with Ar^+ irradiation and the results are compared with those obtained for freestanding graphene. The complexity of the defects can be controlled via the irradiation energy. By combining molecular dynamics simulations with scanning tunneling microscopy, the study shows that with energies starting from 1 keV, the presence of a substrate leads to more complicated defect structures compared to the results obtained for freestanding graphene. At lower energies, the presence of the substrate decreases the defect production, as the metal surface prevents forward sputtering of carbon atoms. At 1 keV, the ion can be channeled in the interface between graphene and the substrate, introducing line-like defects in the lattice by using perpendicularly shot ions.

Publication IV: Ion irradiation of metal-supported graphene: exploring the role of the substrate,

C. Herbig, E. H. Åhlgren, C. Busse, J. Kotakoski, A. V. Krasheninnikov, and T. Michely, submitted for publication.

The work presented in this publication continues the previous work on irradiation response of metal-supported graphene, concentrating on the fate of the carbon atoms sputtered in the forward direction towards the substrate. The study includes experimental work with scanning tunneling microscopy and atomistic simulations using molecular dynamics simulations and density functional theory. Upon annealing, the carbon atoms stuck at the interface form small graphene platelets. The number of atoms taking part in the platelet formation changes with the ion energy and the species. He^+ was found to be the best candidate for defect production without substantial amount of platelet formation with simultaneously presenting a high sputtering yield.

Publication V: Atomistic two temperature modeling of swift heavy ions in freestanding graphene: creating nanoporous graphene,

E. H. Åhlgren, A. A. Leino, F. Djurabekova, A. V. Krasheninnikov, K. Nordlund, S. L. Daraszewicz, J. Kotakoski, in preparation

High energy ions interact with their target mostly through the electronic system. Graphene has a high electric and thermal conductivity, suggesting that the energy deposited on the

target is quickly dissipated into the lattice. Whether any defects are seen in the membrane after swift heavy ion irradiation is already an interesting issue. The defect production is studied with two temperature molecular dynamics, which takes into account the electronic and thermal properties of graphene. The obtained results suggest that defect production is possible and results in circular holes in the membrane. Simulations with various ions and energies produce estimates for the defect production, and the hole diameter can be controlled via the stopping power of the ion.

2.2 Author's contribution

The author carried out the molecular dynamics simulations in publication **I, II, IV** and **V**, in publication **III** those simulations including the substrate. In publications **I, III** and **IV** the author did the analysis of the molecular dynamics data and in publication **IV** participated in the analysis. The author wrote the first draft of the publications **I** and **V** and the draft of the computational part of publication **III**, and contributed in the writing of the classical computational part in publication **IV**.

Chapter 3

Graphene

Graphite is a commonly known carbon material that consists of stacks of graphitic sheets [4], in which carbon atoms are arranged in a hexagonal lattice, piled up on top of each other forming a layered structure bound together by weak van der Waals forces, see Fig. 3.1. The layered structure itself raises a question: How many layers are needed for a stable configuration? It turned out that only a single layer is required [2], a theoretical limit, just one layer of atoms lying on a plane. Such a layer is called graphene. The covalent bonds between the carbon atoms within the plane are much stronger than the weak planar forces keeping the stack piled up. The weak bonding allows the planes to slip relative to each other, thus creating an environment where peeling of layers one by one is possible, a commonly seen procedure while writing with a carbon pencil.

Single layer graphene is also the basic building material for other low dimensional nanomaterials such as nanotubes [5], which can be thought of as a graphene membrane rolled up to form a tube, as well as for fullerenes [6], a single layer rolled to form a ball, although graphene was discovered decades later. The first graphene samples were produced from bulk graphite with thicknesses ranging from few layers down to a single layer [2]. The electronic properties of graphene membranes start to change with increasing amount of layers, gradually approaching the bulk graphite values. But up to how many layers can it still be called graphene? A bilayer graphene has almost the same electronic properties as a single layer, but already with three layers the electronic spectrum is more complicated [7].

3.1 Background

The electronic band structure and conductance of a single layer of graphite was studied theoretically already in 1946 by R. P. Wallace [1]. Forty years before the name 'graphene' was first introduced by Saito et al. [8]. The nature of this still purely theoretical material started to reveal. Graphite itself is a

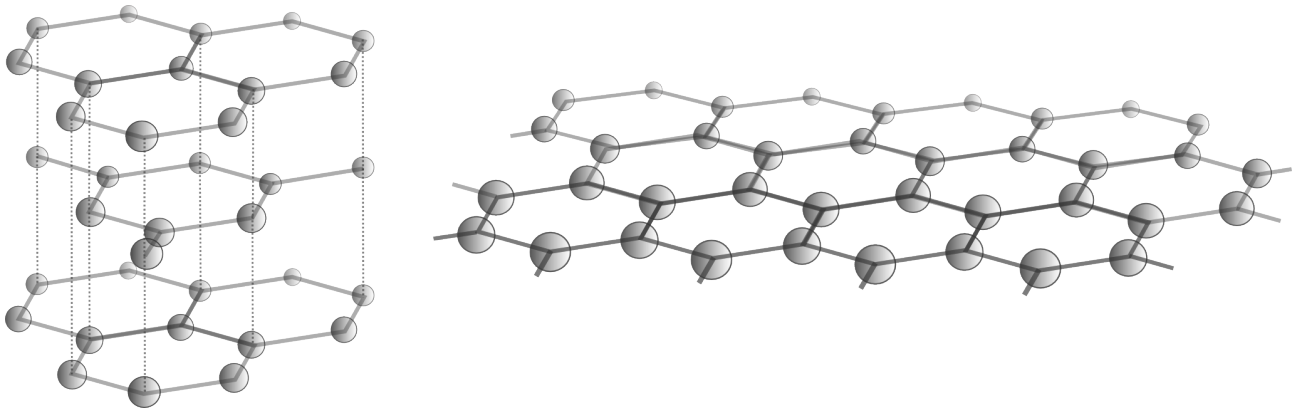

Figure 3.1: Schematic illustration of the atomic structure of graphite. By isolating one layer, graphene is obtained.

metal, but with a reduced number of atomic layers, the semiconducting nature could be lured out to the daylight. Other theoretical studies confirmed these predictions, and continued in these footsteps diving deeper into the peculiar features of the graphite layers including studies on the magnetic behavior during the next decades [9–12]. The field of carbon allotropes got a boost in the 80's as fullerenes and carbon nanotubes were set into the limelight as stable nanosized structures [5, 6]. Tunable electronic properties and low dimensions were some of the appealing features that suggested that these materials could be suitable for electronic applications developed by industry. As a highly conducting two-dimensional material, graphene could be thrown in the same category. The only problem was, stable samples of monolayer graphene were still regarded as daydreaming among the experimentalists. Scientists continued to study the theory, considering smaller fragments of graphitic sheets, graphene nanoribbons, where the edge shape was found to change the electronic states and introduced new features [13, 14]. These edges can be thought as defects, which implied that if graphene could be manufactured, its electronic properties could be tuned by controlling the defects in the atomic structure. A single atomic layer of graphite was still unreachable for scientists. How could something as thin as one layer of atoms exists in a planar form rather than roll up like nanotubes and fullerenes did?

After years of pursuit, the first stable monolayer of graphene was obtained in 2004 [2], paving the way for graphene nanoelectronics. Six years later it led to the greatest tribute a physicist can be awarded, a Nobel prize. The study used a surprisingly simple method that required graphite, adhesive tape and a microscope. The first graphene samples that resulted in the remarkable reputation of the material were obtained by peeling of a mesas of highly oriented graphite. Simple as that. The samples obtained were no bigger than a few micrometers, but were undeniably stable in ambient conditions.

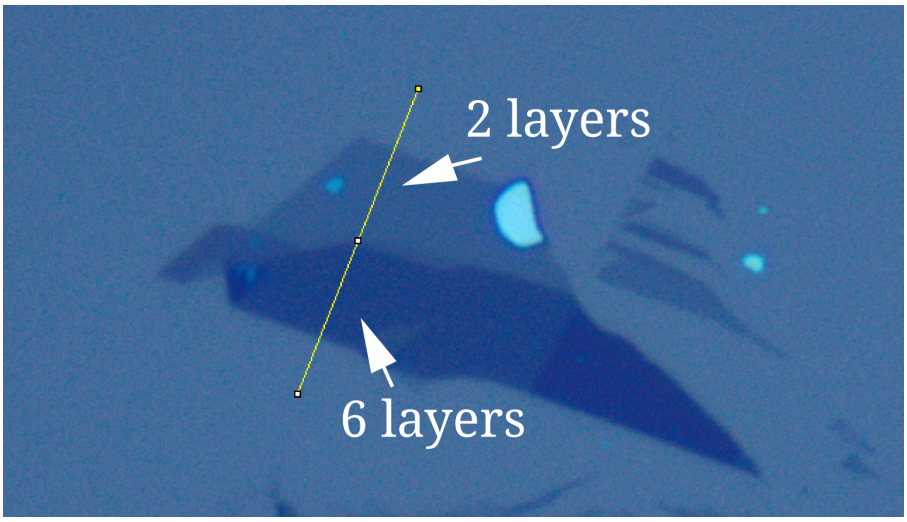

Figure 3.2: A typical graphene sample obtained by peeling of graphite with tape. The sample is placed on top of oxidized metal, and identified with an optical microscope. The thickness can be determined by the amount of light that passes through the sample. A single layer of graphene absorbs about 2.3% of the reflected light. The visible thickness contrast is due to the phase shift of reflected light. By measuring the intensity of the light at different parts of the sample, the thickness can be determined. Image courtesy of Franz Eder.

3.2 Synthesis of graphene

The research on graphene has been expanding after it was successfully produced in 2004. Soon more effective methods for manufacturing the material were introduced [15]. The methods can be divided into three categories: mechanical and chemical preparation, and growth. Mechanical preparation includes the formerly mentioned tape-method, in which highly oriented graphite is peeled off layer by layer until the thickness of one atomic layer is obtained. The samples are then identified using an optical microscope [16], see an example of a peeled sample in Fig 3.2. This method is cheap, and in principle, easy to apply, but sample sizes are small (micrometers) and random, and the preparation process tedious. The obtained samples are often single grain, which means that the crystal lattice consists of a single continuous crystalline domain without grain boundaries. The second category cosists of the chemical preparation which can be done by oxidation-reduction. Graphite oxide has oxygen containing groups on the carbon planes and the exfoliation is done under water with ultrasonication [17]. This results in graphene layers which still have some residual functional groups left. It is cost efficient and produces hydrophilic samples, but because of the residual oxygen, the method is not as appealing as others and still under development.

On the other hand, the third group includes the growth methods, which are suitable for large scale manufacturing of graphene, and produce multi-grain crystals. The principle behind this method was

invented already in the 20th century. Chemical vapor deposition [18, 19] is a method in which a substrate material is exposed to a hydrocarbon gas such as benzene, which provides the needed carbon. The growth requires a suitable temperature depending on the substrate surface's reactivity. The growth can be controlled layer by layer and the sample sizes are up to centimeters with crystalline domains up to micrometers in size [20, 21]. This category also includes a method where graphene layer can be grown by doping a substrate material with carbon atoms, which then segregate to the surface of the sample by annealing, and form a continuous graphene network on the substrate's surface [22]. The thin layer can be then removed from the surface and transferred to a desired platform for further use. The samples used in the experimental studies presented in publications **III** and **IV** were grown by adsorption of ethylene on a clean Ir(111) surface, resulting in good quality samples.

3.3 Mechanical properties

In addition to the remarkable feature of being only one atomic layer thick, graphene has other properties that derive from its unique crystal structure. Moreover, the difference to bulk materials must be taken into account. The quantities describing bulk materials can not be directly compared to those values of 2D graphene. The strain energy density is normalized by the area of the sheet, not the volume, as in the case of traditional 3D materials, resulting in units of force/length. These can be converted into values corresponding to the parameters of 3D materials, by dividing them by the interlayer distance of graphite (0.335 nm). However, these values should be used only to compare graphene's properties with the ones of bulk materials, as the values are not intrinsic attributes of the single layer membrane.

Elastic behavior of a material under axial extension can be described as $\sigma = E\epsilon + D\epsilon^2$, where σ is the stress, ϵ is the strain, E is the Young's modulus and D is the third-order elastic modulus [23]. Young's modulus describes the material's elasticity or stiffness along the axis where the stress is applied in the elastic regime, and the third order term gives the nonlinear elastic response. More accurate calculations include nonelastic terms even up to fift-order with fourteen independent elastic constants [24]. For a single layer of graphene, nanoindentation measurements yield a 2D Young's modulus of about 340 N/m, a third-order term of about -690 N/m and intrinsic strength of about 42 N/m. The corresponding 3D values are 1.0 TPa for Young's modulus, -2.0 TPa for the third-order term and 130 GPa for the intrinsic strength at a strain of 0.25 [23]. The values vary with the quality of the sample, as presence of defects and grain boundaries lower the strength of the material [25–27]. For comparison, the Young's modulus of a polycrystalline diamond film is about 530 GPa [28] and the tensile strength of an ideal diamond is about 95 GPa [29]. These values show the virtue of graphene: It is almost twice as stiff as diamond and outmeasures even the ideal diamond in strength. Not to

get too mesmerized by the mechanical characteristics, graphene cannot withstand compression as the membrane is free to buckle as the compression is applied.

3.4 Electronic properties

The electrons of the carbon atoms are distributed in three distinct states. The lowest *1s* state includes two electrons as do the other two states, *2s* and *2p*. Three electrons from the two higher states, two from *2s* and one from *2p*, are responsible for the bonding between the carbon atoms in graphene, each carbon atom having three bonds, creating the so called σ band. This results in the peculiar bond length of 1.42 Å in graphene [30], and accounts for the sp^2-hybridization, i.e. the mixing of the atomic orbitals, as the $2s$ orbital is mixed with two $2p$ orbitals. The last electron in the *p* state forms the π band which has also one empty site, and gives graphene its electrical conductance properties.

The electronic band structure of graphene was first modeled by P. R. Wallace in 1947 [1]. The approach uses the tight-binding approximation for the electrons at the π orbital of graphene, treating electrons as a set of wave functions originating at the location of each atom. It takes into account the nearest and the next nearest neighbor interactions with the π orbital electron, but neglects the overlapping of the wave functions. The model was improved in 1998 to include the overlapping for the nearest neighbors. It describes the electronic energies at the symmetry point **K** correctly, discussed in the next section, but further away more accurate models are needed, such as analytical methods taking into account up to three nearest neighbors [31].

The electronic band structure depicts the electronic conductance of a material. Materials with no band gap are considered metals, and those with the gap either semiconductors or insulators, depending on the size of the gap [32] . The size is described by the amount of energy that is required to excite electrons over the gap from the valence band to the conduction band, see Fig. 3.3 . Within the gap the density of states, meaning the number of states that electrons can occupy in a certain energy range, is zero. Graphene is frequently considered a semimetal as the valence and conduction bands are connected at one point, called the **K** point [33–35]. The symmetry point **K** is rather unique among materials. It is the point in the band structure where the valence and conduction band touch, thus there is no band gap at that point, and the electrons in the π band can easily excite to the conduction band, see Fig. 3.3 for the band structure. Around the symmetry point, the slope of the bands is linear, which leads to a high velocity of the charge carriers $v_F \approx 1 \times 10^6$ m/s called the Fermi velocity. Contrary to usual cases, in graphene the Fermi velocity does not depend on the energy or the momentum of the particle itself.

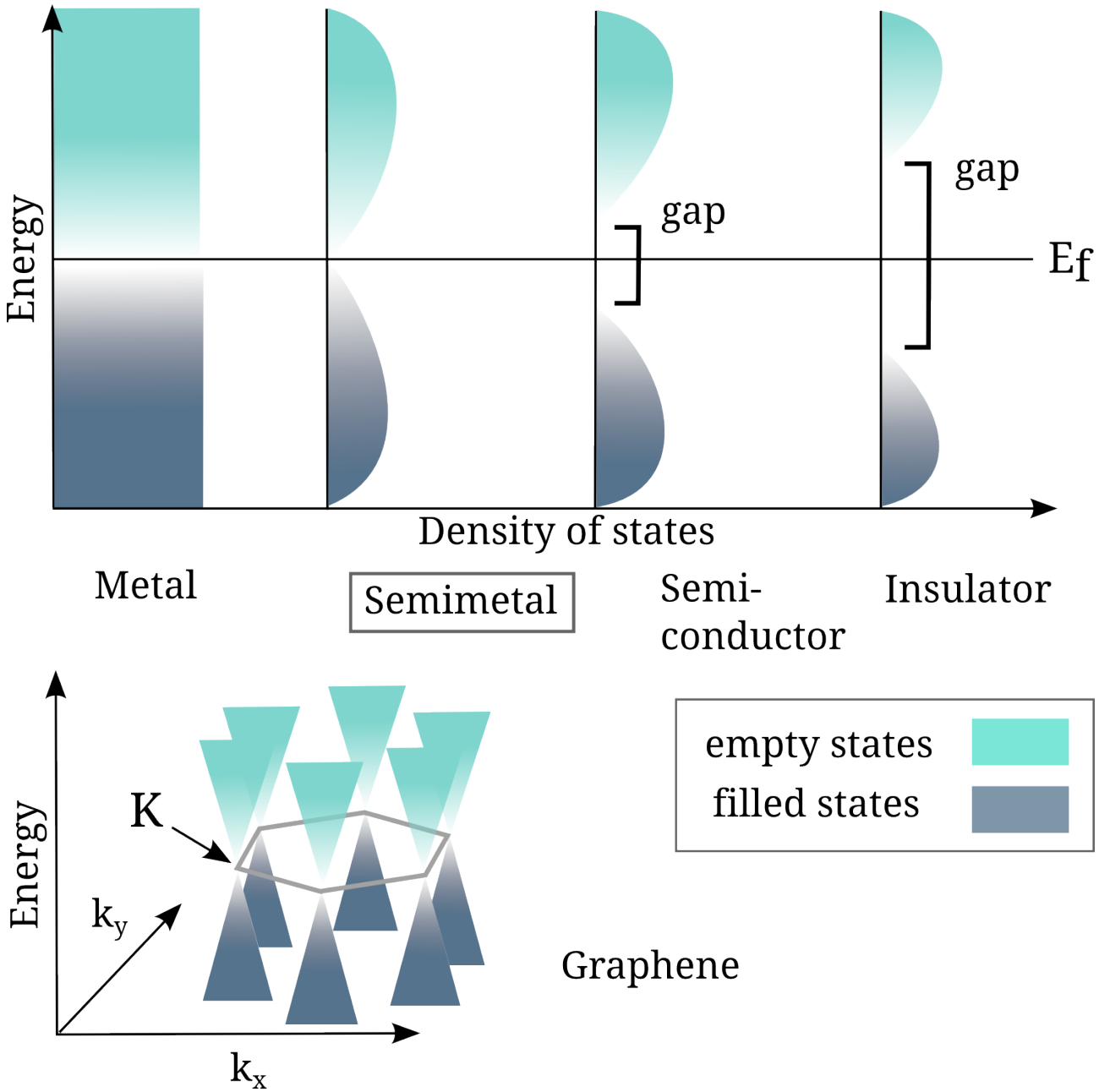

Figure 3.3: A schematic presentation of the electron band structure of a metal, semimetal, semiconductor and an insulator, showing the full (blue) and empty (green) states in the valence and conduction bands. The vertical line represents the Fermi energy, where there is a theoretical 50% probability of a state to be filled or empty at equilibrium, whether there is a state or not at that point. The band gap is shown for the semiconductor and insulator, while for semimetal and metal there is no gap. As shown in the lower part of the figure where energy is plotted against the reciprocal space vectors $\mathbf{k_x}$ and $\mathbf{k_y}$, graphene is a semimetal with the valence and conduction band touching at the **K** point with linear slopes.

3.5 Controlling the properties of graphene

For these interesting properties to be of any use in the real life applications, a tool is needed to precisely modify the atomic structure and hence the properties of the material. Introducing dopants in a material is a standard way to modify the material's electronic properties in semiconductor industry. Increasing or decreasing the number of electrons in the lattice can lead to n-type or p-type behavior of the material, respectively. In n-type materials the lattice has an increased number of electrons which act as charge carriers, whereas in p-type materials the amount of electrons is decreased and holes are the dominant charge carriers. In the case of graphene, the defects introduced in the lattice have a strong effect, changing its properties from a semimetal with no band-gap to a semiconductor with a tunable gap [36–39]. For graphene, the natural dopants are boron (B) and nitrogen (N), which have exactly one electron less and more than carbon that has a total of six electrons, respectively. The electron structures are for B: $1s^2 2s^2 2p^1$, C: $1s^2 2s^2 2p^2$, and N: $1s^2 2s^2 2p^3$. B and N are comparable to carbon also in terms of size, which eases their incorporation into the graphene lattice, where they can replace carbon atoms.

There are several methods to dope a material. These often require gas treatments and precursors as well as high temperatures to enable the chemical reaction. Boron doping can be done e.g. by pyrolysis of boron-containing polymeric precursor and hydrogen physisorption [40] or selective exposure to multiple elements including boron, nitrogen and hydrogen [41]. For nitrogen, the doping can be done by adsorption of molecules such as NO_2 on top of graphene [42]. Some methods require pre-existing vacancies that can then be filled with nitrogen during NO treatment [43]. What is common for these methods is that most of them require high temperature, a precursor, multiple gases and they lead to inhomogeneous doping and even possible contamination of the sample. Ion beams provide a precise tool for doping, avoiding most of the aforementioned fuss, as studied in the work presented in this thesis.

Defects in the lattice also change the mechanical properties of the material. Vacancies in the graphene lattice has been shown to significantly drop the mechanical properties of graphene [44]. On the other hand, the defects do not affect the 2D elastic modulus and the breaking strength of the material. Nevertheless, if defects are created in a precise manner, the patterns may be useful for specific applications, such as cutting the membrane to a specific form or creating porous graphene for thin filters.

Chapter 4

Methods

4.1 Ion irradiation

Regarding the nanometer-sized scale of graphene, one cannot take a pair of scissors to cut the structure and be done with it. No, a far more sophisticated tool is needed, a tool that enables one to modify the material on the atomic scale, one atom at a time. Luckily the silicon based semiconductor industry has already solved this problem. It has used ion beams since the 70's for etching, surface processing and on the other hand, also for modifying the sample's atomic composition.

The energetic ions of the beam can modify the graphene sheet by knocking atoms away one by one, as discussed in publication **I**. With a right combination of energy and incident ion, the nature of the defect can be predicted. The ions can also be deposited in the target, replacing the original atoms by different species or adding extra atoms, and therefore, adding electrons or holes in the target. Depending on the desired modification, small (including one to few atoms) and large defects (tens of nanometers) can be created in graphene in a controllable way.

The principle with ion beams is that the direction of accelerated charged particles can be controlled at a nanometer-size precision. The particles are first charged positively by tearing electrons away. The charged particles can then be accelerated and focused by large magnets towards the target. The ion species, charge and energy are chosen according to the purpose of the experiment and the facilities in use.

As the ion penetrates the solid, it loses energy every time it undergoes collisions with the target atoms. The interactions of the ion with the solid can be divided into two categories by the nature of the interaction: nuclear and electronic. The nuclear collisions describe the interaction between the positive nuclei of the atoms as elastic collisions. The electronic collisions, on the other hand,

describe the interactions between the electrons of the colliding atoms. In these collisions, energy is transferred to the electron cloud. The interaction mechanisms can vary between these two from being fully nuclear or electronic, to a mixed one. During the irradiation, the deposited energy can also be transferred between the two subsystems.

The strength of the interaction is usually described by a quantity called stopping power $S_{e,n}$, where e and n denote the electronic and nuclear systems. Its magnitude depends on the atomic number of the ion and its energy, as well as of the species of the target atoms. It is quantified by the energy loss ∂E of the projectile per unit distance ∂x traveled in the target material,

$$S_{e,n} = \frac{\partial E_{e,n}}{\partial x}. \tag{4.1}$$

What makes it problematic in the case of graphene and other nanosystems, is that the energy loss is defined per distance traveled in the target material. Graphene is only one atomic layer thick, so the energy loss happens when the ion passes the only atomic layer. Some of the energy of the ion is transferred to the lattice, but as some of the lattice atoms may be detached from the structure, energy will be lost. In publication **V** the stopping power is scaled in order to describe the properties of graphene by dividing it with the interlayer distance of graphite, in a similar manner as the mechanical properties are scaled for enabling comparison with conventional 3D materials, discussed earlier. Regarding the energy of the ion, it has a huge impact on the interaction.

The energy of the incoming ion sets the stage for the main interaction mechanism between the ion and the target atoms. At low initial energy the ion collides with the target atoms creating defects by knocking the atoms on its path. When the energy of the ion increases, the interaction time between the ion and the target atoms get shorter and the ionic collisions are too fast to cause deformation in the lattice. This is when the electronic interactions take the leading part in the play. Some of the energy of the ion is transferred to the lattice by the fast electrons which can excite the electrons of the lattice. The high energy ions, whose interactions are governed by the electrons, are often called swift heavy ions.

Swift heavy ions can create tracks of structural modification in materials [45]. The high energy of the ion introduces high thermal energy to the lattice locally at the path of the ion. This energy transfer causes cylindrical tracks of amorphous material in the solid, which can then recrystallize. The interaction is dominated by the inelastic excitation of electrons of the target atoms. Due to the high energy, the electronic stopping dominates over the nuclear stopping. Though, the exact track formation mechanism is still debated [46] and the mechanism vary with the target material. For insulators

the Coulomb explosion mechanism has been suggested [47]. In it, the ion creates a positively charged region, after which the repulsion between the positive ions causes them to move quickly away from the track to the surrounding lattice. Other mechanisms include the inelastic thermal spike [48], where the projectile ionizes the target atoms along its trajectory. This leads to highly charged lattice ions, and the electrons can then excite secondary electrons. After the charge neutralizes, the temperature starts to rise along the track. The relaxation of the lattice causes the energy of the electronic system to transfer to the lattice atoms. This effect is the so called thermal spike. A repulsive force is induced between the ions and a track is formed in the solid. Other suggested methods include structural relaxation methods [49], which describe the relaxation of the excited electrons to the equilibrium state after the irradiation event. The main mechanism to transport energy from the electrons to the lattice is via electron-phonon coupling. Swift heavy ions on graphene have been studied only for a short time in a few experimental studies [50, 51]. In publication **V** of this thesis, the process is studied using the inelastic thermal spike model.

As explained above, the ion irradiation is a controllable way to create defects in a target material by tuning the ion species, energy and incident angle. The energy of the irradiating ion is the one most important parameter influencing the mechanisms of how the defects are produced. In the low energy range, the emphasis is on the atomic collisions, leading to small defects as only few atoms are involved. At higher energies, the interactions are mainly between electrons, and the effect of the impact is spread in much larger area of the lattice. The resulting defect can include hundreds of atoms. Nevertheless, with any used irradiation energy, the process is too fast for human eyes to observe the details of the impacts.

4.2 Molecular dynamics

As the most fundamental science, the goal of physics is to explain the phenomena in nature, all around us and in the furthest corners of the vast universe. The core of scientific thinking and processing is finding universal laws which explain how things happen in nature as they do. Computer simulations are used to mimic real systems to map a processes not yet experimentally achievable, or to understand what is already seen in the experiments. The motivation for simulating a system or a process comes from nature. Real systems, the role models of their simulated cousins, set a high goal for theoretical calculations.

As the system is only a model from the natural one, the results are not exact. In publications **I-V** results of the molecular dynamics simulations are presented as probabilities for ion irradiation to produce defects in the target material, depending on the type of the incident ion and its energy. A

large number of datapoints is required due to the nature of the simulations, as the point where the ion hits the target lattice affects the results. If the ion always passes through in the middle of a graphene hexagon, the probability of seeing any defects would be really low. By randomly choosing the point of the impact, many of the possible defect configurations are mapped. This way a probability for a certain outcome can be calculated. It gives an estimate of how possible a particular event is for the system.

The computational methods applied in this work are classical molecular dynamics (MD) and two temperature molecular dynamics (TTMD). The methods have been developed to model the time evolution of systems at the atomic scale to provide information on how the atoms move and interact within a system. They act as a computational microscope, opening a view of the system that cannot be achieved with the existing experimental methods.

In classical MD, the positions of atoms are calculated by considering only the ionic interactions, while in two temperature molecular dynamics, the interactions of the electronic system are also included. The reason why the system can be divided into two in the simulations comes from the Born-Oppenheimer approximation [52]. The wave function of a molecule can be divided into two components: nuclear and electronic. The approximation assumes that the movement of the nuclei is slow compared to the surrounding electrons, which allows the electrons to find a ground state configuration for each position of the atoms due to the huge mass difference, and the electronic and nuclear wave functions can be calculated independently. This reduces the number of variables in the calculations significantly. All the MD simulations presented in this thesis are calculated with PARCAS code developed by Kai Nordlund [53].

4.2.1 Algorithm

In MD, the equations of motion of a number of particles are solved numerically by iteration with a finite time step. The method was developed by Alder and Wainwright in the 1950's for studying phase transitions and atomic vibrations in molecules [54–56] and has now gained a steady foothold in the study of atomic scale behavior of matter.

The recipe for a general algorithm goes as follows [57]: First the initial positions for each atom i $\mathbf{r}_i(t_0)$ and velocities $\mathbf{v}_i(t_0)$ are given to the atoms. The positions are chosen according to the studied crystal structure and the velocities are given according to the Maxwell-Boltzmann distribution developed originally for ideal gases, which depends on the mass of the particles and the initial temperature of the system. The second phase includes calculation of the forces $\mathbf{f_i}(\mathbf{r_i})$ acting each atom. With the forces, the new positions $\mathbf{r}_i(t_{n+1})$ and velocities $\mathbf{v}_i(t_{n+1})$ are determined by solving the equations of

motion for an incremental increase of time δt. These can then be used to calculate the new forces. The cycle continues until the chosen simulation time t_{max} is reached.

The equations of motion can be written as

$$\begin{aligned} m_i \ddot{\mathbf{r}}_\mathbf{i} &= \mathbf{f_i} \\ \mathbf{f_i} &= -\frac{\partial U}{\partial \mathbf{r_i}}, \end{aligned} \tag{4.2}$$

where i is the index of the atom, m_i is the mass of the atom and U is the potential energy from where the forces can be calculated, obtained from fitted potentials, which are the topic of chapter 4.2.3.

4.2.2 Two temperature model

The name two temperature MD comes from the two subsystems: the ionic (lattice atoms) and the electronic one. The model calculates separately the electronic temperature (T_e) and ionic temperature (T_i) with two separate heat diffusion equations in local equilibrium. The energy is thought to diffuse cylindrically from the track of the ion, and the radial distance from the track r is included in the equations. The energy exchange is taken into account through the electron-phonon coupling term $G\left(T_e - T_i\right)$ in the diffusion equations [48]

$$C_e T_e \frac{\partial T_e}{\partial t} = \frac{1}{r}\frac{\partial}{\partial r}\left[rK_e\left(T_e\right)\frac{\partial T_e}{\partial r}\right] - G\left(T_e - T_i\right) + A\left(r,t\right), \tag{4.3}$$

and

$$C_i T_i \frac{\partial T_i}{\partial t} = \frac{1}{r}\frac{\partial}{\partial r}\left[rK_i\left(T_i\right)\frac{\partial T_i}{\partial r}\right] - G\left(T_e - T_i\right), \tag{4.4}$$

where C is the specific heat capacity, K the thermal conductivity and T the temperature, r is the radial distance from the trajectory and t is the time. The subscripts e and i denote the electronic and ionic subsystems, respectively. $A(r,t)$ is the radial energy distribution of secondary electrons per unit time as described by Waligorski [58].

In the combined two temperature molecular dynamics model, the ionic system evolves by molecular dynamics, while the electronic system is solved from the diffusion Eq. 4.3. The two subsystems are divided into electronic and ionic temperature cells with a typical width of about 10 Å. The energy exchange between the electrons and the ions is due to the electron-phonon coupling term, which is included in the diffusion equation of the electrons and in the modified equations of motion for the ions [59]

$$m_i \frac{d^2\mathbf{r}_i}{dt^2} = \mathbf{F}_i + \sigma m_i \mathbf{v}_i, \tag{4.5}$$

with

$$\sigma = \frac{\frac{1}{n}\sum_{k=1}^{n} GV_N(T_e^k - T_i)}{\sum_i m_i(\mathbf{v}_i)^2}, \tag{4.6}$$

where, m_i and $\mathbf{r}_i$ are the mass and position of atom i, $\mathbf{F}_i$ is the force acting on atom i, $\mathbf{v}_i$ is the velocity of atom i, V_N is the volume of a cell and the summation is done over all atoms in that cell. The last term in Eq. 4.5 introduces the electron-phonon coupling in the equation.

4.2.3 Models for atomic interactions

The used potential is the key ingredient in the simulations. In describes the interactions between the atoms and therefore controls the evolution of the system in the simulation. In classical theory, the interactions between macroscopic systems can be described by the Newtons equation $m_i\ddot{\mathbf{r}}_\mathbf{i} = \mathbf{f}_\mathbf{i}$, as described in Eq. 4.2. For microscopic system at the atomic scale, the electrons of the system affect the interactions and a quantum mechanical approach is needed. The wave function describing an atom can be written with the Schrödinger equation [60]

$$i\hbar\frac{\partial}{\partial t}\psi = H\psi, \tag{4.7}$$

where i is the imaginary number, $\hbar$ is a constant, t is time, ψ is the wave function of the atom and H is the hamiltonian describing the total energy of the particle. Solving this at each time step of the

simulation for all of the atoms would require heavy calculations. Heavier than what is computationally possible at the moment. Therefore, other methods have been developed for modeling the interactions.

Density-functional theory

This method described next was used mainly in publication **IV** by the collaborators and is now briefly introduced in order to provide the needed information to understand the presented results.

As the interactions between the nuclei and the electrons can be described in detail by density-functional theory (DFT), it is rather heavy regarding the computational time needed, and therefore, used mainly for small systems. Often the purpose is to find the ground state electron density for a specific system. The electrons of a system are not considered individually, which would result in a many-body problem of N electrons and $3N$ spatial coordinates, but as a density giving only three spatial coordinates. The Hohenberg-Kohn theorems [61] are used to determine the ground state energy of a many-body system. The system is described by electron density in an external potential that describes the locations of the nuclei in the system following the Born-Oppenheimer approximation. The energy that minimizes the energy of the functional is the ground state energy of the system. The ground state energy of an interacting electron gas in a static potential $U(\mathbf{r})$ can be written as

$$E = \int U(\mathbf{r})n(\mathbf{r})d\mathbf{r} + \frac{1}{2}\int\int \frac{n(\mathbf{r})n(\mathbf{r'})}{|\mathbf{r}-\mathbf{r'}|} + G[n], \tag{4.8}$$

where the $n(\mathbf{r})$ describes the electron density, and $G[n]$ the universal functional density. For an interacting electron gas $G[n] = T_s[n] + E_{xc}[n]$. The first part describes the kinetic energy of the non interacting electrons with density n, and the second part describes the exchange correlation energy of the interacting system with density n. The functional form of the $E_{xc}[n]$ is generally not known, but if the density of the system varys only slowly, it can be approximated by $E_{xc}[n] = \int n(\mathbf{r})\epsilon_{xc}(\mathbf{r})d\mathbf{r}$, where ϵ_{xc} is the exchange and correlation energy of a electron gas of density n. This is called the local density approximation (LDA), and it gives almost exact solutions for systems with slowly varying n. Further approximations are used in order to e.g. reduce the interactions between the particles using pseudo potentials to describe the core electrons of atoms [62].

Analytical potentials

For large systems, the quantum mechanical approach is too heavy. To enable calculations with increased computational efficiency and allow handling of systems including millions of atoms, analytical potentials are used to describe the interactions between the atoms. The quantum-mechanical electronic structure of the system is approximated by analytical functions. These functions are constructed and fitted to describe the behavior of the atoms observed in experiment or in quantum mechanical calculations.

One of the simplest analytical potentials is the pair potential. The potential energy of the system depends only on the interatomic distance of the atom pair. An example of this is the Morse potential [63], which includes two terms

$$U(r) = D\exp\left(-2ar\right) - 2D\exp\left(-ar\right), \tag{4.9}$$

where D and a are constants and is r is the interatomic distance. The first term describes the repulsive part of the interaction, which is dominant at short distances and describes the Pauli repulsion of overlapping electron orbitals as well as the Coulomb repulsion of the nuclei. The second term describes the attractive part, which is stronger at larger separations, and decays to zero for long enough distances, see Fig 4.1.

A need for a more complex potential arises for describing covalently bonded crystal structures such as graphene, where the direction of the bond must be taken into account. The Tersoff potential [64, 65] takes into account the strength of the bond (bond order) which depends on the local geometry of the lattice i.e. the neighboring atoms. The bonds of an atom with multiple neighbors are weaker than the bonds of an atom with only few neighbors. The potential sums over atom pairs i and j to yield the total energy of the system E in a similar manner as the pair potential

$$E = \sum_i E_i = 1/2 \sum_{i \neq j} U_{ij}, \tag{4.10}$$

where

$$U_{ij} = \left[A\exp(-\lambda_1 r_{ij}) - B_{ij}\exp(-\lambda_2 r_{ij})\right]. \tag{4.11}$$

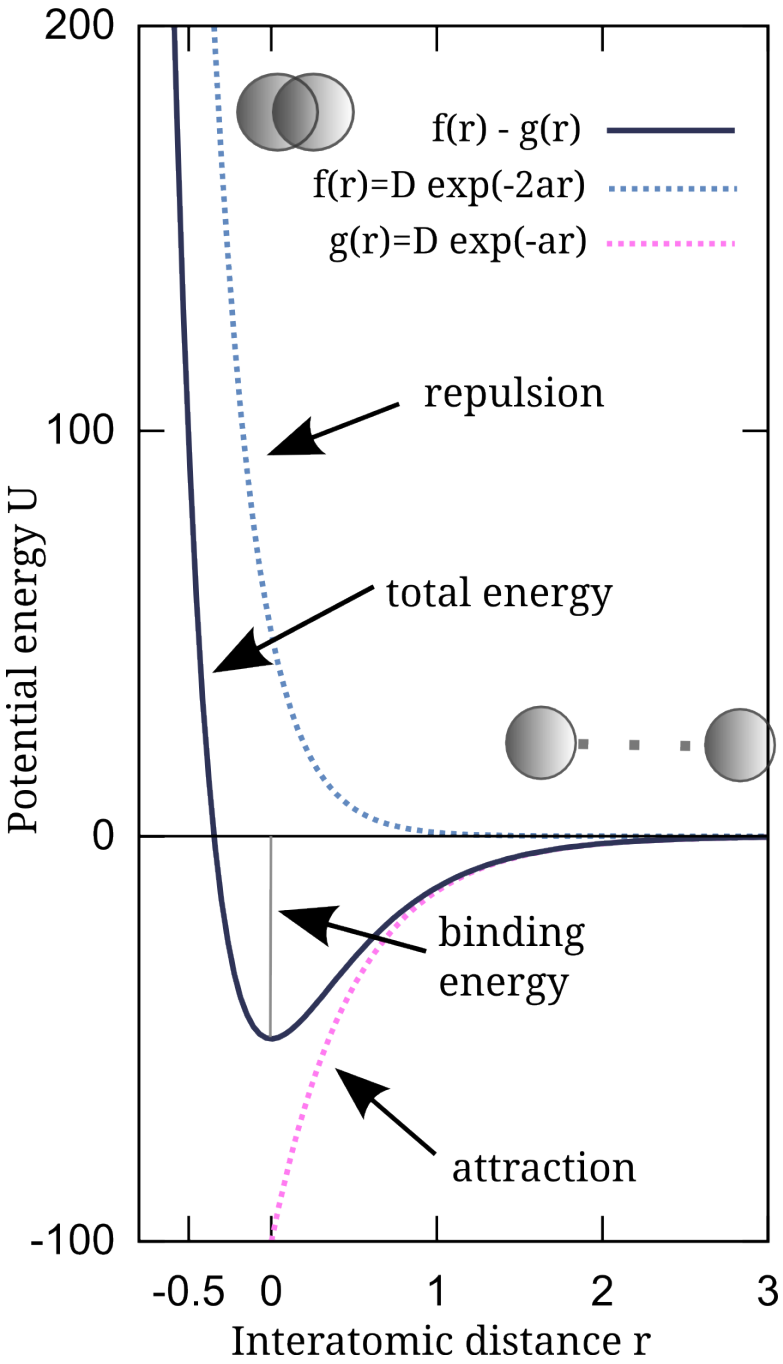

Figure 4.1: The attractive and repulsive parts of the interaction between two atoms according to the Morse potential. The resulting total energy of the system, and the binding energy of the atoms at equilibrium distance, are indicated.

Here the first term inside the square brackets is a repulsive pair potential and the second term describes the attractive part. A, λ_1 and λ_2 are fitted constants. Addition to the simple pair potential comes in the term B_{ij}, which represents a measure of the bond order as a function of the coordination of the atoms

$$B_{ij} = (1 + \chi_{ij})^{-1/2}\,, \tag{4.12}$$

where

$$\chi_{ij} = \sum_{k \neq i,j} f_{ik}(r_{ik}) g_{ik}(\theta_{ijk}) exp\left[2\mu_{ik}\left(r_{ij} - r_{ik}\right)\right], \tag{4.13}$$

and

$$g(\theta) = \gamma\left(1 + \frac{c^2}{d^2} - \frac{c^2}{d^2 + (1 + cos\theta)^2}\right). \tag{4.14}$$

In Eq. 4.13, $f_{ik}(r_{ik})$ is a cut-off function limiting the range of the potential, θ is the bond angle between atoms i, j and k, and μ is a constant, as are γ, c and d in Eq. 4.14.

In publications **I-V** the carbon-carbon interactions are modeled with the reactive Tersoff-type potential by Brenner [66, 67], and in the publication **I** the boron-carbon and nitrogen-carbon interactions are modeled with the Tersoff-type potential by Matsunaga [68].

The repulsive interactions of the energetic ions and the target atoms is described by a potential by Ziegler, Biersak and Littmark [69]. It is smoothly joined to the Tersoff-type Brenner potential discussed above, to describe correctly the energetic collisions of the atoms at short atomic separations [70].

4.2.4 Special conditions regarding irradiation simulations

Fast, high energy collisions between the atoms set special requirements for the simulations. The most important of these are discussed in the following.

Boundary conditions

In the atomic scale, natural systems are huge. Even though in MD simulations the systems can include millions of atoms, the sizes are small compared to macroscopic systems. There is just not enough computational capacity to study macroscopic systems in detailed atomic level. The solution to this problem is periodic boundaries. This method treats the opposing sides of the system as continuous over the edges, therefore creating an infinite system.

The smallest scale, to give an absolute minimum for the system size, is the cut-off distance of the potential. It is the distance within the interactions of the neighboring atoms are calculated. To ensure realistic system dynamics, and to avoid taking the atoms into account multiple times, the explicit simulation box size must be larger than twice the cut-off distance. If the box size is too small for the chosen cut-off distance, the interactions are taken into account multiple times, leading to unrealistic behavior of the system.

Temperature and pressure control

The equations of motion that govern the course of the simulations conserve the total energy of the system. During the simulation, large amounts of energy can be deposited on the target atoms in a short time. For a system with periodic boundaries, the deposited energy does not leave the system, and ends up increasing the kinetic energy of the atoms and possibly resulting in an explosion of the system. If the system is assumed to be a part of a larger macroscopic system, almost infinite when looking at it at the atomic scale, it gives the added energy a possibility to dissipate to a larger system resembling a heath bath. In the target structure within the simulation box boundaries, this can be mimicked by a thermostat which is coupled to a few atomic rows at the system edges. In the publications the Berendsen thermostat [71] is used to scale the velocities of the atoms at the periodic edges towards a temperature T_0 with equation

$$\frac{dT}{dt} = \frac{T_0 - T}{\tau}, \tag{4.15}$$

where T is the temperature of the system and τ is a time constant. In the simulations presented in this thesis, the temperature T_0 was set to zero Kelvin at the system edges. By choosing a large enough system-size, the effects of the thermostat to the simulation results can be minimized.

Similarly for pressure, the Berendsen barostat scales the simulation box vectors, which describe the size of the simulations system. The pressure changes towards a pressure p_0 while the volume of the simulation box can fluctuate according to

$$\frac{dp}{dt} = \frac{p_0 - p}{\tau}, \tag{4.16}$$

where p is the pressure of the system and τ is a time constant. The pressure control is applied in all publications included in this thesis, while relaxing the initial structure prior irradiation to reach the minimum energy configuration.

Adaptive time step

In the simulations, a time step is chosen to define how often the interactions between the atoms are calculated. For particles moving with high velocities, the equations of motion must be calculated frequently, at the expense of computational efficiency. In the publications included in this thesis, the time step is varied according to the particles moving with the highest velocity, maintaining the computational efficiency and ensuring that the atoms do not jump between positions too coarsely even if the velocity of the particles changes drastically.

The time step can be adjusted during the simulation by making it inversely proportional to the recoil atom velocity, the product of the total force experienced by the recoil atom and its velocity, and ensuring that the value of the time step does not increase over 10 % from its previous value according to [53],

$$\delta t_{\mathrm{new}} = \min\left(\frac{k_t}{v_{\mathrm{max}}}, \frac{E_t}{v_{\mathrm{max}} \times F_{\mathrm{max}}}, 1.1 \times \delta t_{\mathrm{old}} \times \delta t_{equilibrium}\right), \tag{4.17}$$

where k_t, E_t are constants, v_{max} is the velocity of the atom and F_{max} the maximum force experienced by any atom in the system. δt_{old} and $\delta t_{\mathrm{equilibrium}}$ are the previous and equilibrium time steps, respectively.

4.3 Scanning tunneling microscopy

In the experimental part of the work presented in publications **III** and **IV**, our experimental collaborators have used scanning tunneling microscopy (STM) to image nanosized objects at atomic resolution. The accuracy of it is in the scale of single atoms. The main idea behind this method is outlined here.

STM, developed in the 1980's by Binning et al. [72], is a nondestructive method to probe the surface of even the smallest samples. The microscope has a narrow conducting tip, which is placed on top of a sample close to the surface. A bias voltage is applied between the sample and the tip, which leads to quantum mechanical tunneling of electrons between these two. If the voltage is kept constant, the tunneling current changes and depends on the distance between the tip and the surface. On the other hand, if the tip is kept at a constant distance from the surface, the voltage changes according to the electron density of the sample surface. This information can often be interpreted as a direct image of the atomic structure of the surface.

Chapter 5

Ion irradiation effects in graphene

5.1 Low energy irradiation of freestanding graphene

5.1.1 Ion doping

The doping of a material fills its purpose only if the structure of the material is not otherwise changed. Therefore, studying other defects along with the dopant configurations is important.

Publication **I** addresses the ion beam doping of freestanding graphene with boron and nitrogen ions. The irradiation damage is studied by applying molecular dynamics simulations with varying ion energies at the low energy region between 10 eV and 4 keV. At this energy range, the interactions between the ion and the target atoms are ionic in nature, as discussed before in section 4.1. The low energies ensure that the created defects are precise and point-like, including only few atoms, and the ion is more likely to stop at the membrane rather than cause large defected areas.

The study shows the typical defect configurations in graphene after the irradiation. The frequently seen defect types are substitution, where exactly one carbon atom is replaced by B or N, substitution with a neighboring vacancy, single vacancy formation, and double vacancy formation. At low energies the B and N atoms can settle on top of otherwise intact graphene as adatoms. The ion can also pass through the membrane without causing any defects, or bounce back in the direction where it came from. A schematic illustration of the defects is shown in Fig. 5.1. The probabilities for each defect configuration were calculated and are discussed below.

Substitutional defects are created when the ion can transfer enough energy to the target for one atom to be sputtered, as the ion itself is stopped and it takes the place of the displaced atom. Substitution of carbon atoms with N ions is most probable with the ion energy close to 50 eV, indicating the most

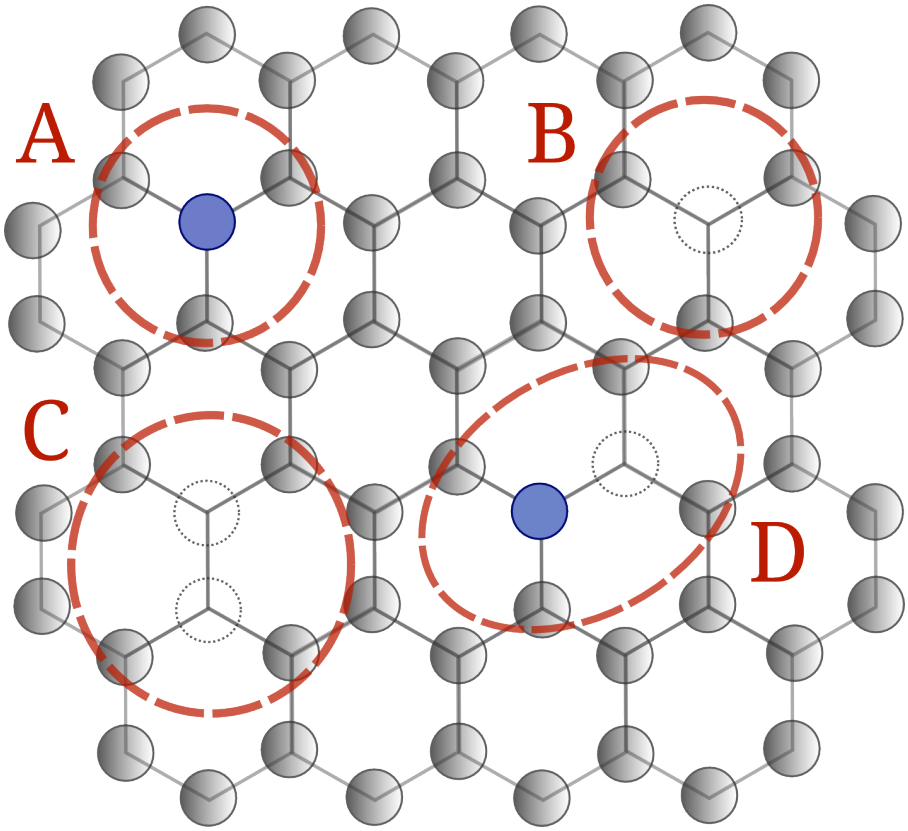

Figure 5.1: Schematic illustration of the simplest defect types in graphene a) substitution, b) single vacancy formation, c) double vacancy formation and d) substitution with a neighboring vacancy. The dotted circles denote the missing atoms.

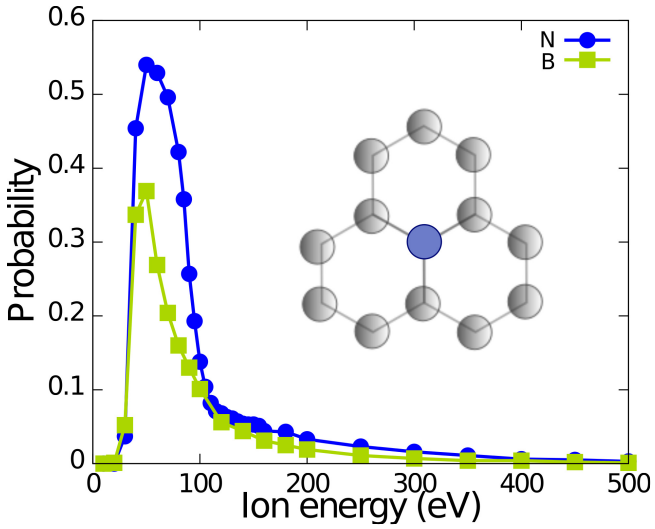

Figure 5.2: Probability for a B and N substitutions in graphene as a function of the ion energy. From publication **I**.

suitable energy for N doping. At this energy over half of the simulation cases produce a substitution of carbon with N. The probability displays a single peak as a function of the ion energy, as shown in Fig. 5.2. The energy needed for a carbon atom to be displaced from graphene is about 20 eV for a head-on collision [73], though, this type of a direct impact is unlikely as there is much free space in the lattice. Most of the impacts are not direct and require more energy to displace a carbon atom. For B the maximum probability is lower, slightly below 40%, also displaying a single probability peak at energies slightly below 50 eV, see Fig. 5.2. The lower substitution probability of B can be explained partly by the size difference of B and N. With a bigger atom, the effective area of the collision, which leads to the displacement of a target atom, is larger. For energies higher than 100 eV, the probability for B and N ions to be incorporated into the lattice drops, and only few atoms are added to the lattice. At these energies other defect types are more common, as discussed later.

The substitution defect is not always perfect, it is also seen with a neighboring vacancy. This defect complex forms as the ion first displaces two carbon atoms from the graphene, then takes the place of one of the carbon atoms. For an ion to be able to displace two carbon atoms simultaneously, enough energy needs to be transferred to the lattice, requiring higher initial energy compared to the case of a perfect substitution. There are two paths that lead to this defect. The first one is traveled by N: the ion sputters both of the two displaced carbon atoms with a single impact, and stops itself at the graphene sheet. In the second path, taken by lighter B, the ion is first scattered in the in-plane direction, sputtering one carbon atom, after which it hits another carbon atom and takes its place. The probabilities for this dopant-vacancy complex formation are low, and less than 4% of the impacts lead to this configuration at any energy, see Fig. 5.3. The difference in probability for N and B is mostly

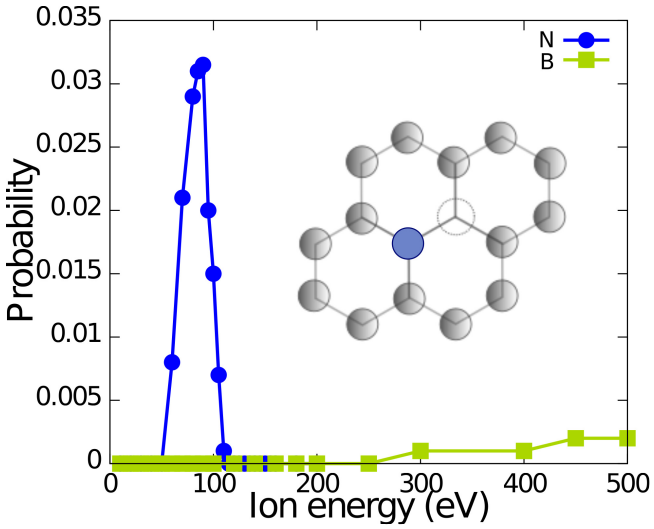

Figure 5.3: Probabilities for dopant-vacancy complexes formation for B and N ion as a function of ion energy. From publication **I**.

due to the mass difference of the ions. N is heavier than carbon and can displace two carbon atoms at a relatively low energy (50-100 eV), while B is lighter than carbon and requires higher initial energy.

With energies below the threshold of sputtering any carbon atoms, the ion can take a dopant site in the graphene without defecting the initial lattice. The ion is attached to the pristine graphene as an adatom, if it does not pass through in the middle of a hexagon or bounce back. The probability for adatom formation is high at low energies, exceeding 70% at energies below 40 eV as shown in Fig. 5.4. The migration barriers for B and N ions in graphenic surfaces range between 0.1-1.1 eV [74, 75], which allows these ions to migrate into possible vacancies present in the lattice, creating perfect substitutions.

In addition to the dopant atoms incorporated into the graphene lattice, there are other types of defects seen during the irradiation. These include defects such as single vacancies, double vacancies and other more complex defects. Publication **I** shows that single vacancy formation has two probability maxima, one narrow peak at lower energies, and an other broader peak at higher energies, see Fig. 5.5. For N the narrow peak occurs at the energy of about 125 eV and the broader peak has a maximum at 400 eV. The probability for B displays the narrow peak at 80 eV and the broader peak maximum at about 180 eV. The highest probability for N is within the narrow peak, about 55%, and for B within the broad peak, about 35%. The narrow peaks can be explained by a chemical interaction between the ion and the displaced carbon atom. The ion forms a dimer with a carbon atom and pulls the carbon with itself. N being heavier than carbon, the effect is more distinguished with N compared to B. For a double vacancy, the maximum probabilities are much lower, 16% for N and 6% for B at the energies of 110 eV and 70 eV, respectively, shown in Fig. 5.5.

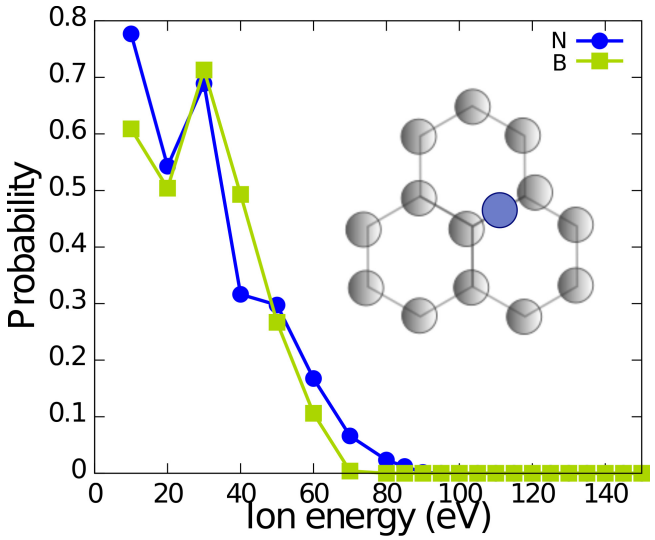

Figure 5.4: Probabilities for B and N adatom formation as a function of ion energy. From publication **I**.

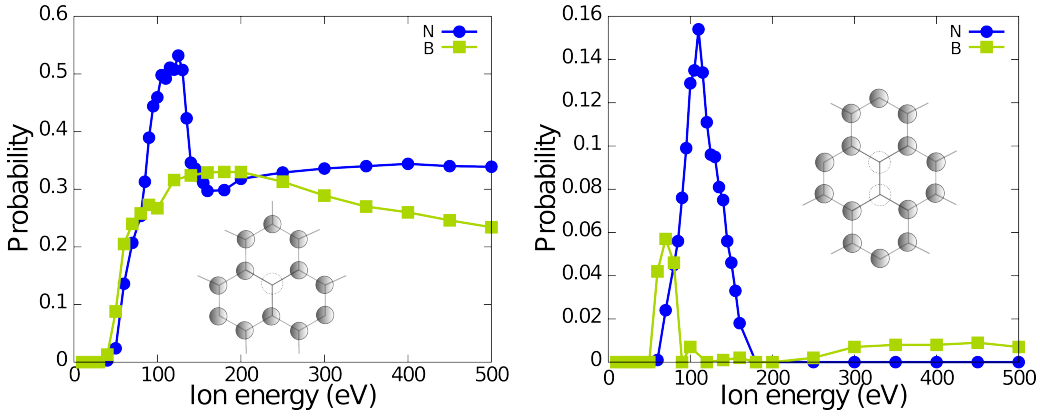

Figure 5.5: Probabilities for single and double vacancy formation by B and N ions. From publication **I**.

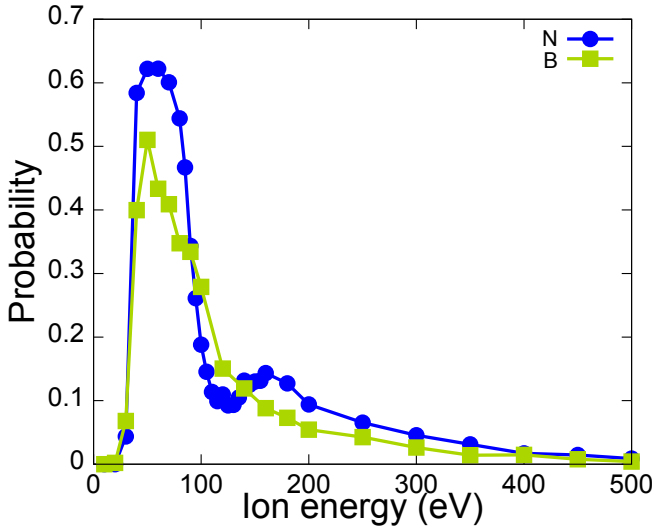

Figure 5.6: The relative probabilities for B and N substitution are shown as a function of the ion energy. From publication **I**.

For an actual irradiation experiment aiming for doping of the material, one needs to combine the data discussed above in order to introduce the desired amount of dopants with a preferably low rate of other defects. The maximum probabilities for a perfect substitution are at about 50 eV, and for single vacancy formation, the most frequent defect type among other defects than substitution, has the highest probability at energies above 100 eV. Therefore, the production of single vacancies and more complex defects occurs mainly at higher energies than substitution. In Fig. 5.6, the relative probabilities for B and N substitution are shown. The figure shows the ratio of sum of probabilities for different substitution cases to the sum of probabilities for all defects for B and N as a function of ion energy. The probabilities peak at about 50 eV, indicating the suitable doping energy. By combining irradiation with two separate energies, one at about 50 eV, and other at lower energies, the deposited low energy dopant atoms would ensure that vacancies created during the irradiation could be filled by the adatoms during annealing.

These simulation results on low energy doping of graphene have been verified experimentally. Bangert et al. [76] reported successful doping of a perfect single layer graphene, confirming the predictions of our calculations. They used 25 eV B and N ions to substitute carbon atoms from graphene. The low energy of the doping ensured that also adatoms were introduced, and those could then fill the possibly created vacancies. This precise, controlled doping is a clear indication of the possibility of industrial scale processing of 2D materials for device applications using existing methods.

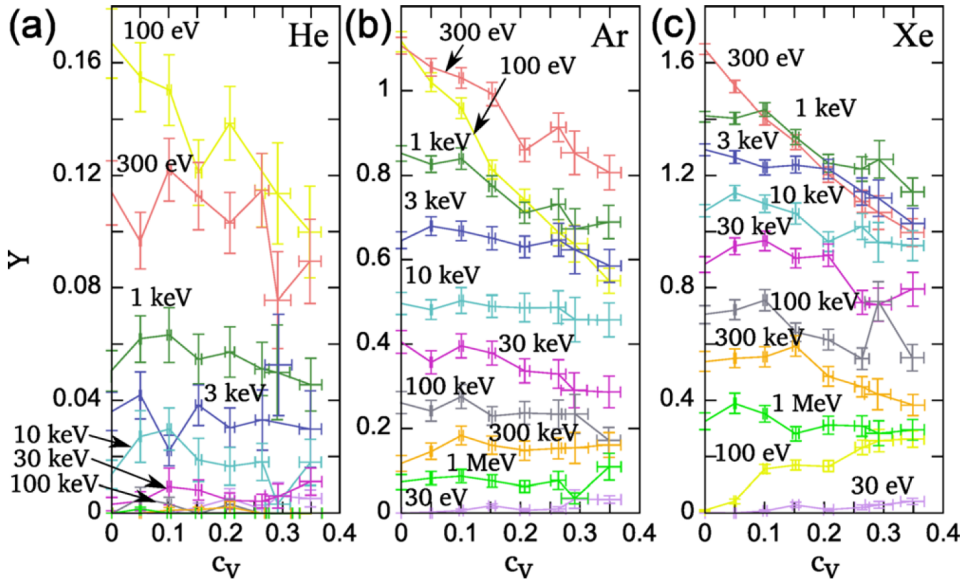

Figure 5.7: The sputtering yield as a function of the vacancy concentration for different ion-energy pairs a) He, b) Ar and c) Xe. From publication **II**.

5.1.2 Radiation tolerance under continuous irradiation

With low ion energies and doses, the created defects are often simple and, as discussed above, highly controllable. As the amount of impacts in the target increases, the defects start to dominate the structure. In its pristine form, graphene is considered as one of the strongest material ever measured [23], and a single layer can withstand the pressure of macroscopic amount of gas [77] as well as keep the smallest atmospheric particles from penetrating it [78, 79]. The defects created by energetic ions are not always desired. When the material is used in conditions where continuous irradiation is present, such as in space or as a part of an ion beam systems to separate high vacuum from a target that is volatile or must be kept in ambient conditions, the durability of the material is highly important. In publication **II** the effect of continuous irradiation on graphene is considered.

To study the defect accumulation, the chosen ions are noble gases which interact only repulsively with the carbon atoms in graphene. The results show that monolayer graphene with a vacancy concentration of at least 35% is stable, and does not show any signs of failure of the structure and full break-up of the membrane. The calculated sputtering yield Y varies with the vacancy concentration c_V and the ion energy. The data displays a decreasing trend for the yield with increasing vacancy concentration due to the increasing probability for the ion to pass through an existing vacancy, see Fig. 5.7. The sputtering yield follows a simple geometric model, where Y decreses with c_V, as the target density decreses and the collision cross section drops. The yield can be written as

$$Y_{c_V} = (1 - c_V)Y_0, \tag{5.1}$$

where $Y_0 = Y(c_V = 0)$ corresponds to pristine graphene. To include the energy dependence into Eq. 5.1, a dimensionless variable γ is introduced,

$$Y_{c_V} = (1 - \gamma c_V)Y_0. \tag{5.2}$$

Fitting Eq. 5.2 to the data in Fig. 5.7 gives values for γ at different energies. In Fig. 5.8 a) Y_0 is plotted as a function of the ion energy, corresponding to $\gamma = 1$. In Fig. 5.8 b) and c) the fitted γ is plotted as a function of the ion energy.

Depending on the value of γ, the irradiation response has different features. For $\gamma = 1$ the model is the simple geometric model shown in Eq. 5.1, and the results correspond to the irradiation of pristine graphene without defects. When $\gamma = 0$, the equation gives a yield that does not depend on the vacancy concentration, i.e. the number of sputtered atoms would be the same if there were defects in the membrane prior to the irradiation or not. Negative values for γ indicate an increasing number of sputtered atoms for increasing c_V, this means that more carbon atoms sputter as the number of vacancies in the membrane increases. Positive values for γ gives decreasing yield for increasing c_V, which means that there is less sputtered carbon atoms as there is more vacancies in the membrabe.

Fig. 5.8 displays negative values for γ at low energies, up to about 30 eV for He and Ar, and 100 eV for Xe, indicating an increasing amount of sputtered atoms for increasing vacancy concentration. With these low energies, close to the displacement threshold of pristine graphene, about 22 eV, the collision cross-section of the ion is large and the time for the ion to interact with the target atoms is long. The lowered binding energy of the carbon atoms in the defected graphene sheet outweighs the lowered target density. With slightly higher energies, between 100 eV and 300 eV, the $\gamma = 1$, corresponding to the simple geometric model and the irradiation of pristine graphene. At these energies, the recoil atoms gain more energy during the collision process and the weaker binding of the lattice atoms is not significant anymore. With even higher energies, the ion sets the recoil atoms moving in the in-plane direction where they can cause secondary collisions. The density of the target does not affect the sputtering yield as much anymore, and γ decreases towards a constant saturation value.

The saturated values of γ are as follows: He 1.08 $\pm$ 0.62, Ar 0.32 $\pm$ 0.10 and Xe 0.53 $\pm$ 0.05. Considering Eq. 5.1 and 5.2, these values can be used to predict the irradiation damage during the

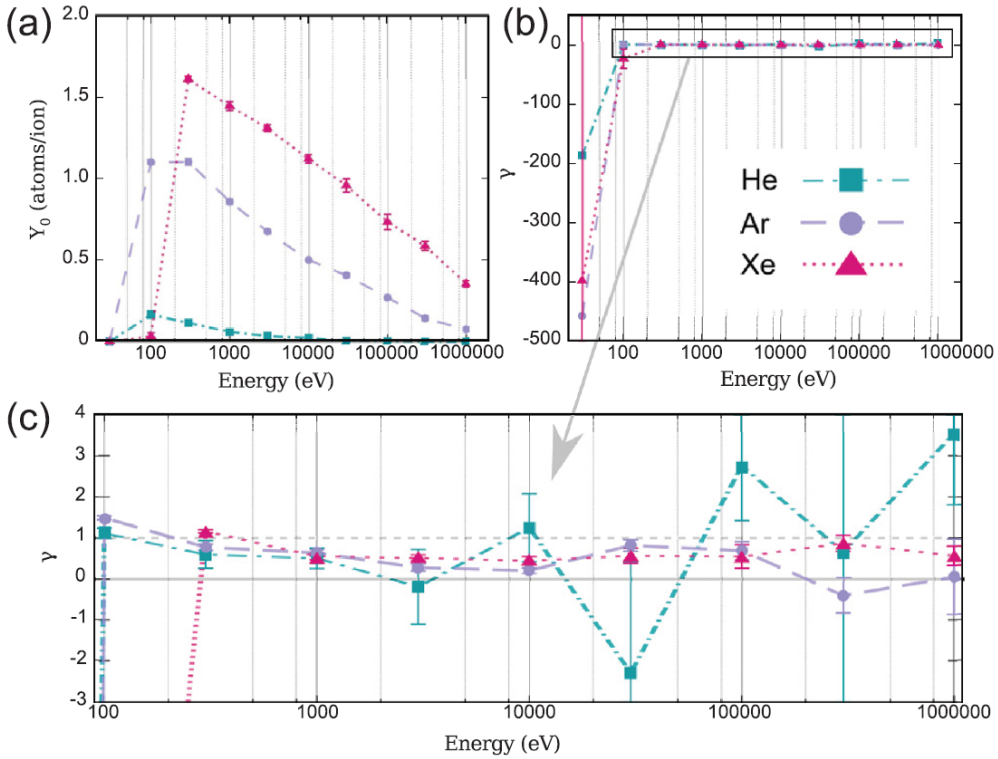

Figure 5.8: a) Sputtering yield for $\gamma = 1$, which corresponds to the sputtering yield of freestanding graphene with zero vacancy concentration. b) Fitted γ as a function of the ion energy, displaying deviation from the simple geometric model. c) Magnification of the marked area from panel b). From publication **II**.

experiment to evaluate whether the created damage is still under the critical amount for the membrane to fit the requirements of the experiment. Now, by applying the method of accumulated damage, the effect of the pre-existing defects to the total sputtering yield and damage production can be better understood.

5.2 Substrate effects on damage production

Keeping in mind that in most practical applications graphene is often resting on a substrate, controlled tuning of the material on a substrate with ion beams is a technologically relevant research question [80–82]. This chapter includes results presented in publications **III** and **IV**. Both publications study the role of the substrate in ion irradiation of supported graphene. Publication **III** concentrates on the comparison between supported and freestanding graphene using Ar^+ irradiation, while publication **IV** includes detailed analysis on the specific characteristics of the substrate-graphene interface area, and the atoms trapped within this region during and after irradiation with Xe^+.

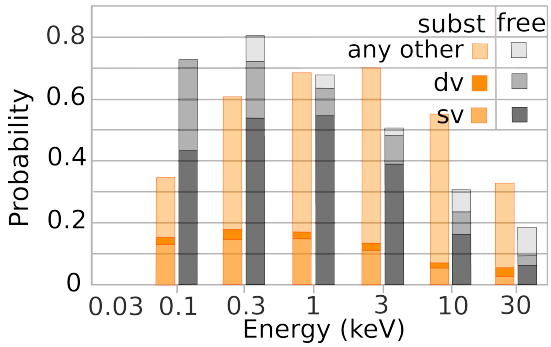

Figure 5.9: Defect probabilities in freestanding (free) and supported (subst) graphene: single vacancy (sv), double vacancy (dv), and other (any other) vacancy formation as a function of the ion energy. From publication **III**.

5.2.1 Irradiation induced damage in freestanding vs supported graphene

On average ion irradiation with the substrate leads to more complex defect structures in graphene. On one hand, the substrate acts as an additional surface where atoms can reflect back, and on the other hand, it acts as an additional source of sputtered atoms which then can contribute to the defect production in graphene. Due to the ion impact, the graphene sheet is pushed towards the substrate and carbon atoms with open bonds can bind to the metal surface contributing to the defect production. The increased amount of defects is seen especially at energies between 1 keV and 10 keV for Ar ions, see Fig. 5.9. The recoil atoms from graphene have enough energy to sputter surface atoms from the metal substrate, some of which then penetrate through graphene while others have just enough energy to cause disorder in the membrane.

The number of sputtered metal atoms per impact ion, the sputtering yield, is actually very low and only a few metal atoms fully escape through graphene. The sputtering yield for the metal as a function of the ion energy is shown in Fig. 5.10. As a reference, the sputtering yield of the metal was calculated also for a clean metal surface without the graphene sheet on top. The yield shows a clear peak of about 14 atoms/ion at the energy of 10 keV. At higher energies, the recoils have enough energy to penetrate deeper into the bulk which is also seen in the damaging probability of supported graphene as it gets lower with high energies. On the other hand, the sputtering yield of carbon atoms has a maximum at the energy range of 1 keV - 10 keV with a maximum value of over 1.2 at the energy of 10 keV. Comparison with the sputtering yield of freestanding graphene reveals that the substrate has a clear effect on the sputtering yield. For freestanding membrane, the maximum yield of about 1 atom per impact ion corresponds to the ion energy of 0.1 keV, well below the energy where the peak was seen in the case of supported graphene. This means that at 10 keV the sputtered substrate atoms have enough

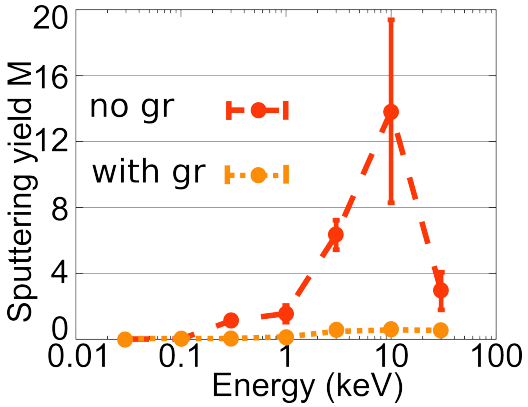

Figure 5.10: Sputtering yield of metal substrate with and without a graphene membrane on top as a function of the ion energy. From publication **III**.

energy to detach carbon atoms from the graphene network from below, but lack the energy to escape themselves.

At low energies, below 1 keV, the substrate actually decreases the damaging probability of graphene. When the ion energy is low enough, the substrate stops the carbon atoms before they are completely detached from graphene. At the energy of 100 eV, all of the defects in graphene are single vacancies, (probability 0.43), and double vacancies (0.3), see Fig. 5.9. Taking the same energy for supported graphene, the single vacancies have a formation probability of only about 0.12, double vacancies about 0.02, and other more complex defects have a formation probability of 0.2 per impact ion. Adding up these numbers yields a total damaging probability for any defect of 0.34 for supported and 0.73 for suspended graphene. The substrate lowers the probability for a defect over 50% compared to the case of freestanding membrane, but the defects are often more complex than pure single and double vacancies. An example of the substrate increasing the damaging probability at higher energies can be found e.g. at the energy of 3 keV. For supported graphene, single vacancy formation has the probability of about 0.11, double vacancy about 0.02 and other defects about 0.57, being the dominant defect type, yielding a total of 0.7. At the same energy for freestanding graphene, single vacancies are the dominant defect type (0.39) followed by double vacancies (0.09), with only a minor contribution from other defects (0.02), giving a total of 0.5. Not only is the probability for creating any defect in graphene on a substrate higher compared to freestanding graphene (0.7 compared to 0.5), but the defects are also more complex (other defects 0.57 compared to 0.02). At the lowest energy studied, 30 eV, no defects are seen, indicating that the energy is too low for the Ar ion to damage graphene.

With a substrate under the irradiated graphene, the ion sometimes gets deflected between those two. The ion travels in the interface area with a sinusoidal trajectory until it has lost enough energy in

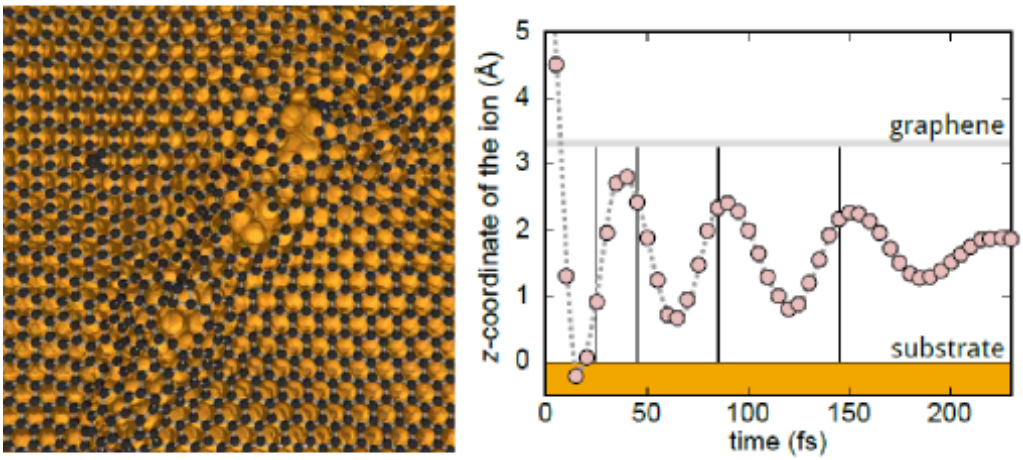

Figure 5.11: Snapshot of a top view of a line defect in the MD simulations after irradiation with Ar^+ at 1 keV. The ion penetrates the membrane and is deflected to the space between the graphene and the metal substrate. Along the way, it produces damage and creates a line-like defect. A schematic illustration of the formation of a line defect with the ion's z-coordinate as a function of time is presented on the right hand side. Reproduced from publication **III**.

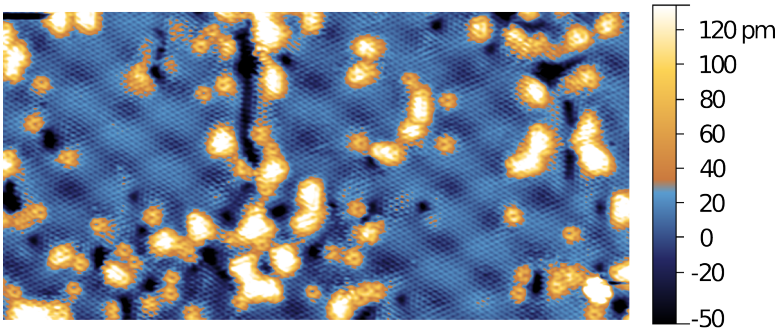

Figure 5.12: STM image on a line-like defect on graphene after irradiation with Ar^+ at 1 keV for 30 s. The image size is 30 $\times$ 14 nm. From publication **III**.

the impacts with the metal surface and the graphene sheet, see Fig. 5.11. Along the ion path a line of small vacancy type defects can be spotted. STM images show these long depression-like features appear after 1 keV Ar irradiation, see Fig. 5.12. The same type of defects are seen in grazing-incidence irradiation with exactly the same formation mechanism [83].

5.2.2 Platelet formation

In a typical irradiation event the ion penetrates graphene and sputters or displaces carbon atoms in the forward direction towards the metal substrate, causing a collision cascade on the metal surface. The impact produces vacancies in the metal surface and bulk, as well as adatoms and small atom clusters

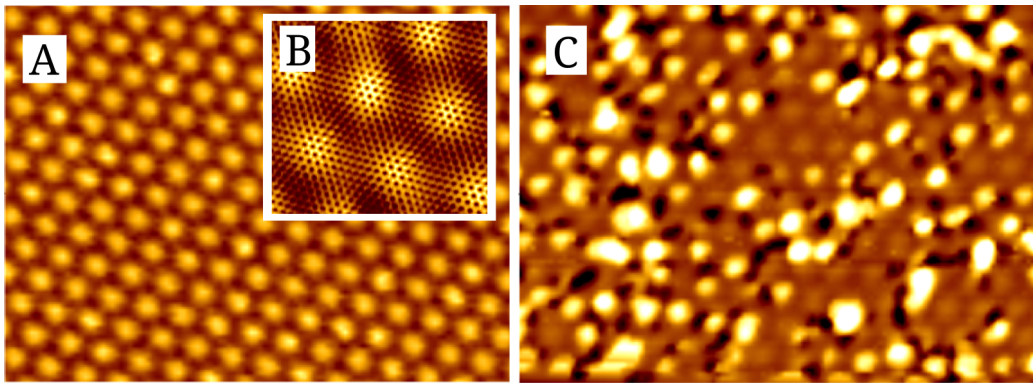

Figure 5.13: A typical STM picture of a) pristine graphene on a Ir(111) substrate, image size is 40 nm $\times$ 30 nm. b) A magnification of the atomic structure on a). The image size is 7 nm $\times$ 6 nm. c) The sample after irradiation with 1 keV Xe^+ at room temperature. From publication **IV**.

on the metal surface. In a STM topograph, two types of features are seen: dark depressions that are interpreted as vacancies or vacancy clusters in graphene with edges bound to the substrate, and bright protrusions which are interpreted as metal adatoms at the interface, see Fig. 5.13. The height of the protrusions indicates that these features actually are due to the metal adatoms, not the carbon atoms. They tend to bind to hcp and fcc threefold hollow sites on the metal and have a lower protrusion hight compared to the carbon adatoms.

After annealing the samples at 1000 K following the irradiation, large bulges with a diameter up to about 8 nm and height of about 3 Å appear in the STM topographs, see Fig. 5.14 for an STM image of a bulge. The graphene membrane appears continuous over the bulge edges. These bulges are interpreted to be caused by graphene platelets forming at the interface. Those carbon atoms that are sputtered in forward direction and implanted in the metal agglomerate to form the platelets. The dark depressions remain visible after annealing but the small protrusion produced by metal adatoms have disappeared. The high temperature provides the metal adatoms the needed kinetic energy to annihilate with the existing surface vacancies, while the noble gas ions are highly mobile under the graphene that is weakly bound to the metal, and can escape through existing holes in the membrane. Only the carbon adatoms are left to form the platelets.

DFT calculations on carbon adatoms show that during annealing, the carbon atoms implanted into the metal tend to segregate to the interface area, allowing them to participate in the platelet formation with other forward sputtered carbon atoms. Diffusion of carbon into the metal is energetically unfavorable, while binding back to graphene membrane requires 6 eV more energy compared to binding to the metal surface. The most favorable lattice site for carbon to adsorb is the hcp threefold hollow site with an adsorption energy of 0.7 eV, the fcc threefold hollow site taking the second place with an energy of 1 eV.

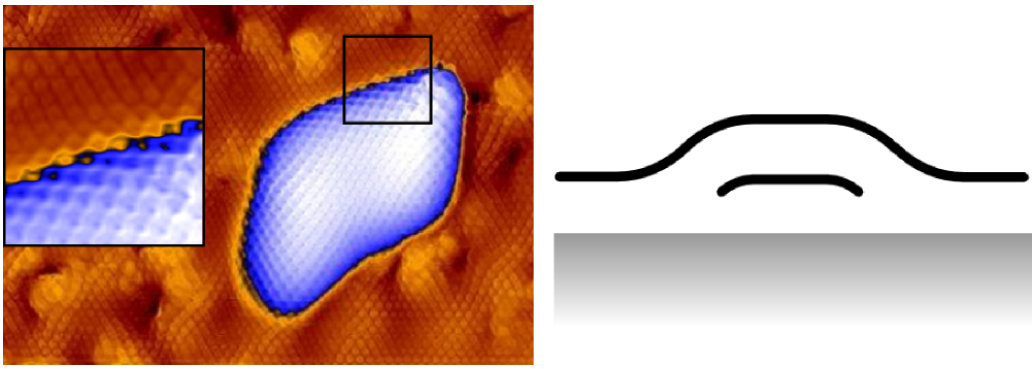

Figure 5.14: A typical STM image of a bulge after irradiation with 1 keV Xe^+ followed by annealing at 1000 K. The image size is 16 nm $\times$ 10 nm. Inset: Magnified view of area indicated by the black square displaying a continuous graphene layer over the bulge edge. A schematic cross-section of a bulge is shown on the right hand side. Reproduced from publication **IV**.

The irradiation induced defects on the metal surface assist the platelet nucleation. DFT calculations for small clusters of carbon atoms in sp^2-hybridized configurations on the metal surface yield a formation energy barrier of 3 eV per atom with a critical cluster size of 5 atoms, after which the formation energy gets lower. For a cluster nucleating on a metal surface step edge, the corresponding critical size is the same, 5 carbon atoms, but the energy is decreased by about 2 eV. This means that the defects on the metal surface offer a nucleation site for the graphene platelets as the metal adatoms annihilate with existing surface vacancies only during the annealing.

In publication **IV** a new quantity is introduced to describe irradiation damage of supported 2D materials, called trapping yield. The trapping yield presents the number of carbon atoms in the interface area between graphene and the substrate after irradiation. The number of trapped carbon atoms varies with ion species and energy. At low energies below 0.1 keV, the momentum transfer from the ion to the carbon atoms is too modest for detaching them from graphene and sending them to the interface area where they can take part in the platelet formation. Momentum transfer increases for higher energies, but the scattering cross section of the collision gets smaller, decreasing the number of detached carbon atoms. This leads to a maximum trapping yield at the intermediate energies around 0.3 - 1 keV, see Fig. 5.15. Simulation results and STM images yield slightly different values for the trapping yield, but display a consistent trend.

The dependence of the trapping yield on the ion species is strong. The yield increases from almost zero for He^+ to about 3 trapped carbon atoms per impact for Xe^+, see Fig. 5.16. The low trapping yield of He^+ combined with a sputtering yield of about 0.2 carbon atoms per impact ion, i.e. approximately every fifth ion sputters one carbon, suggesting that He^+ irradiation can be used as at tool for precise atom by atom modification of graphene lattice on a metal substrate, avoiding the trapping of the

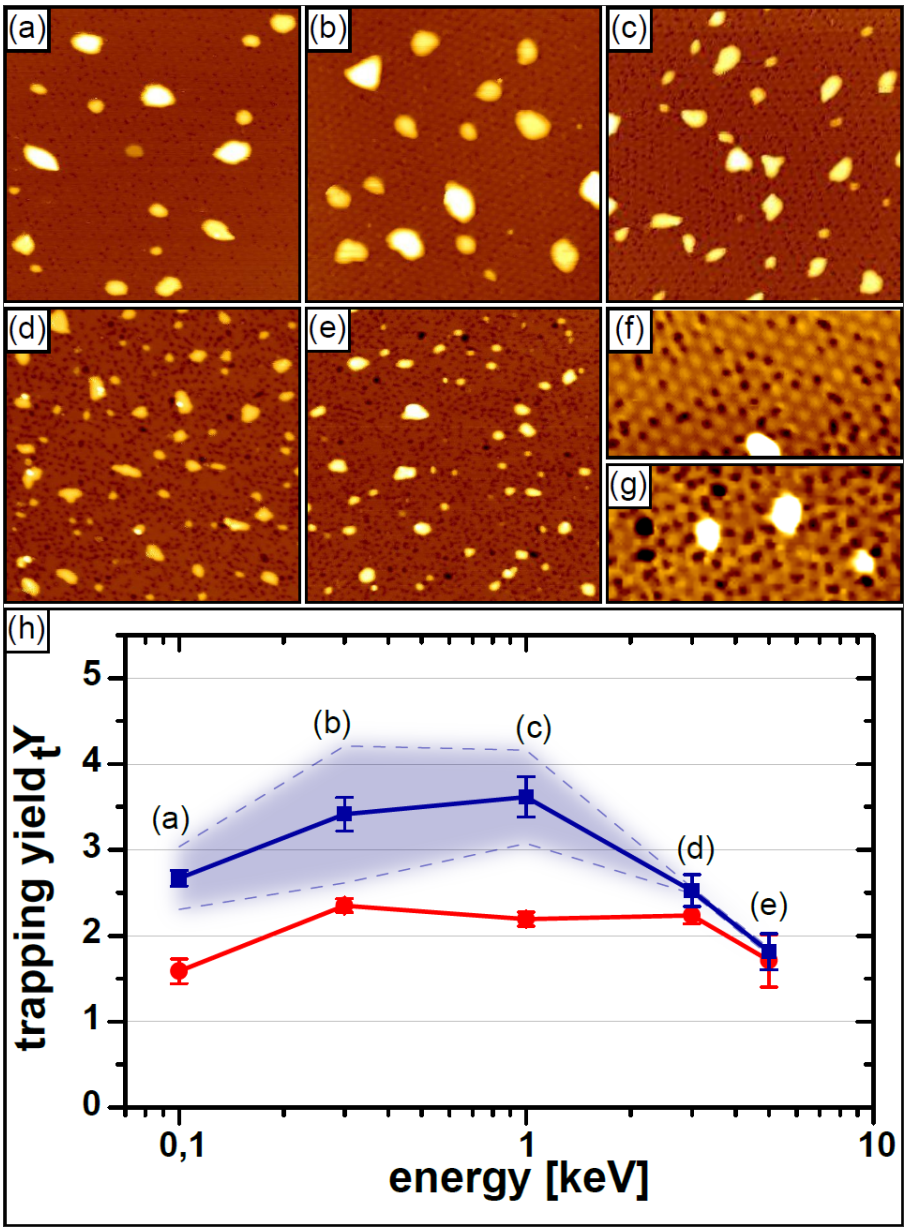

Figure 5.15: Trapping yield as a function of energy with STM images of Xe^+ irradiated graphene on Ir(111) surface after annealing. The energies in a) - e) are indicated in h). The close ups f) and g) are from a) and e), respectively. The image sizes for a) to e) are 80 nm $\times$ 80 nm, and for the close ups 40 nm $\times$ 20 nm. Data from the simulations is marked with red, and from the experiments with blue markers. The shaded area represents the uncertainty in the experiments. From publication **IV**.

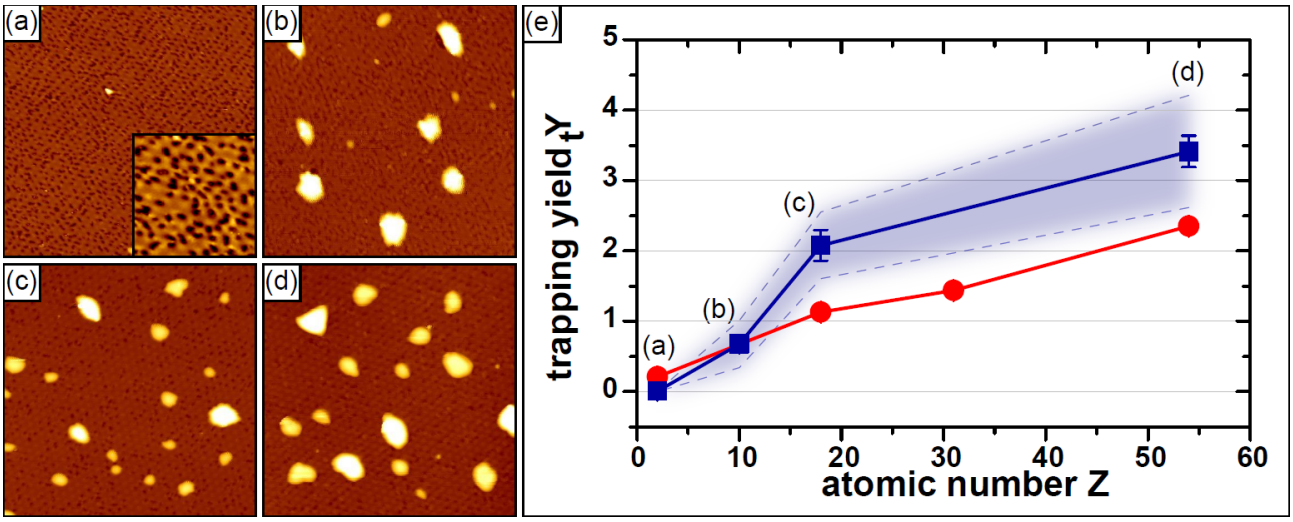

Figure 5.16: a) - d) STM topographs of graphene on Ir(111) surface after irradiation with 0.3 keV ions, and annealing at 1000 K. The atomic numbers of the ions are indicated at e). Image sizes are 80 nm $\times$ 80 nm, and the inset 20 nm $\times$ 20 nm. e) The trapping yield as a function of the atomic number Z of the ion. The values obtained from the simulations are marked with red, and the experimentally measured values with blue, including the shaded area representing the uncertainty in the experiments. From publication **IV**.

carbon atoms at the interface. A panel of snapshots from the molecular dynamics simulations of the irradiation for different ions is shown in Fig. 5.17.

5.3 High energy irradiation of freestanding graphene

Graphene has high electric and thermal conductivity, which suggests that the energy deposited on the target is quickly dissipated into the lattice. Therefore, any defects seen in the membrane after swift heavy ion irradiation at MeV energies is already an interesting issue. This was studied in publication **V** with two temperature MD simulations.

The parameters describing graphene's electronic system during the simulations include the electronic specific heat capacity $C_e(T_e)$, the electronic thermal conductivity $K_e(T_e)$, the electronic stopping power of a projectile $\partial E_{e,n}/\partial x$, and the electron-phonon coupling term g. The electron-phonon coupling is estimated by considering the relation between the electronic specific heat capacity and a relaxation time τ describing the processes involving phonons, as $\tau = C_e(T_e)/g(T_e)$. For graphene, the measured τ for optical phonons has the value of about 150 fs [84]. The obtained electron-phonon coupling constant depends on the $C_e(T_e)$, but neglects the effects of doping and energy level shifting.

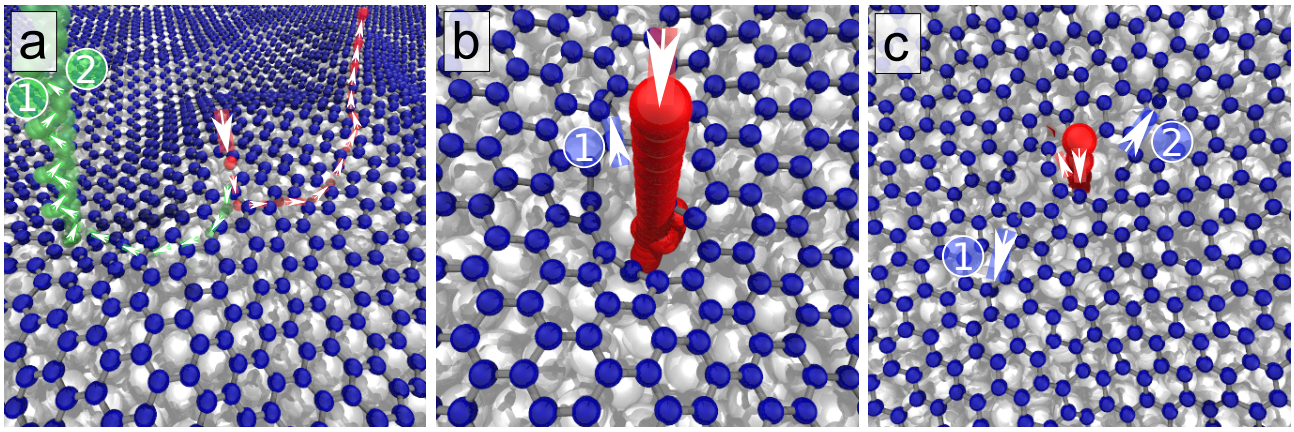

Figure 5.17: Snapshots from molecular dynamics simulations displaying a) a frame of He irradiation at 0.3 keV and 598 fs. The intermediate positions of the ion are shown in red, and that of the two sputtered carbon atoms in green, marked with numbers. b) A frame of Xe irradiation with the same energy at 579 fs. One carbon atom is detached and trapped at the interface (marked with the small arrow and number). c) A frame of 5 keV Xe irradiation at 398 fs. The ion is marked with red. The two detached carbon atoms marked with numbers become trapped. From publication **IV**.

Simulations with different carrier concentrations, calculated by DFT, show that the doping does not affect the results significantly.

There is a wide range of thermal conductivity $K_e(T_e)$ values reported for graphene [85, 86]. The highest ones are around 1400 $\mathrm{Wm^{-1}K^{-1}}$ at room temperature, while at the other end of the range the values are close to 4 $\mathrm{Wm^{-1}K^{-1}}$ at the same temperature. The high conductivity decreases the amount of defects seen in graphene in the simulations. With the highest values no structural changes in graphene are seen for any of the studied ions ranging from He to Ta. Simulations with the low values show that already a slight change in the thermal conductivity leads to 40% change in the defect size. For comparison, Fig. 5.18 presents the hole diameter in graphene after irradiation with different stopping power values. The comparison is made between the lowest studied $K_{\mathrm{min}}(T_e)$ and a slightly higher value $K_{20\times\mathrm{min}}(T_e)$.

The used model is highly sensitive to the thermal conductivity values leading to different defect sizes in the membrane. The approximations made in the model surely affect the results, but even with large errors, the simulations indicate that with the highest reported thermal conductivity values no defects are produced in graphene, which is against of what is observed in the experiments [50, 51]. On the other hand, with the lowest studied conductivity values used $K_{\mathrm{min}}(T_e)$, a hole was always produced in the membrane. Even the ion with the lowest studied stopping power of about 0.74 keV/nm produced a hole with a diameter of about 30 Å. With the slightly higher conductivity values $K_{20\times\mathrm{min}}(T_e)$, the observed defect threshold was set to a stopping power of about 1.3 keV/nm. This corresponds well to the experimentally observed threshold of 1.5 keV/nm [87].

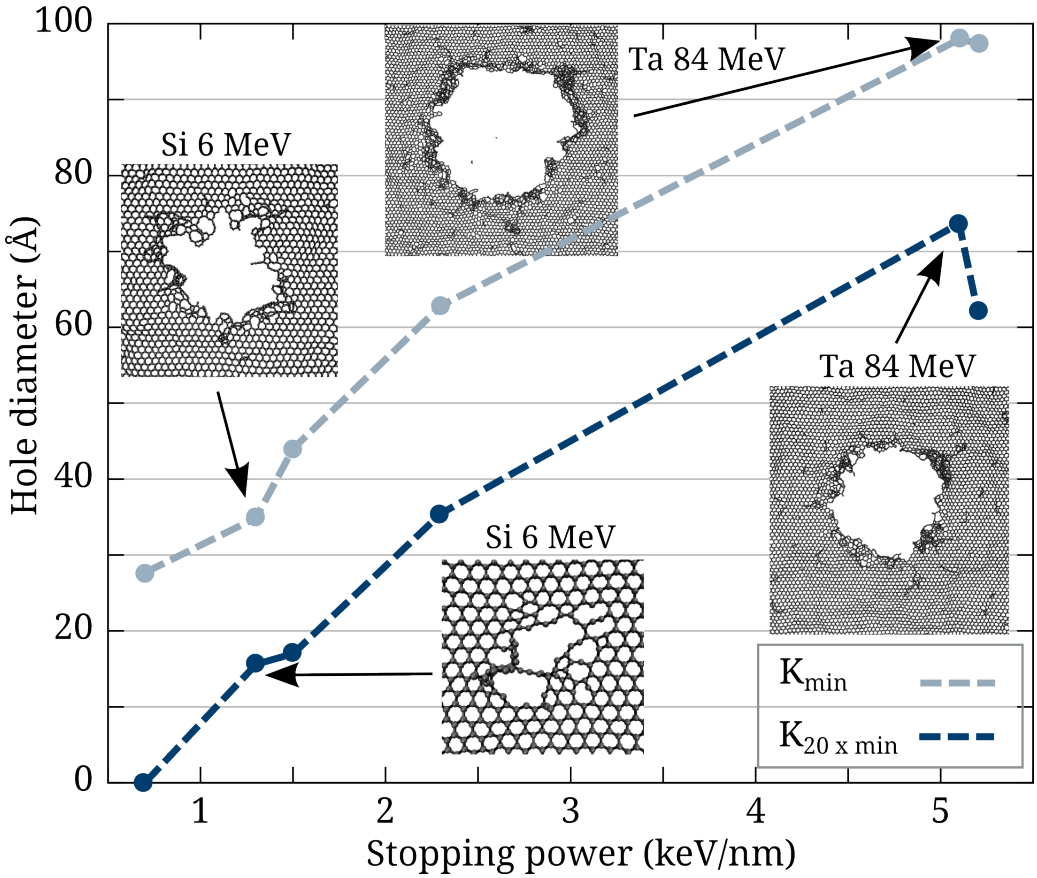

Figure 5.18: The hole diameter presented as a function of the stopping power. Two different low electronic thermal conductivity values $K_{\mathrm{min}}(T_e)$ and $K_{20\times\mathrm{min}}(T_e)$ are compared. From publication **V**.

These results show that even though graphene has high electric and thermal conductivity, electronic interactions during high energy ion irradiation at the MeV range are enough to produce large hole-type defects in the membrane. The diameter of these defects can be controlled with the stopping power of the chosen projectile, and it varies from a few nm to tens of nm's. This type of nanopores could be used in nanodevices designed for e.g. DNA sequencing [88] where the holes in one atomc layer thick membrane offer a highly sensitive detector, or as a porous membrane for gas separation [89–91] and water desalination [92].

Chapter 6

Conclusions

The aim of this thesis is to look into the subject of how ion irradiation could be used to modify the lattice structure of graphene in a controlled manner. Macroscopic materials have been exposed to ion beam irradiation for decades in order to change the properties of the materials. The recipe for this is well established and studied, but the same irradiation parameters do not apply in the nanoscale. In the case of graphene, and other low dimensional materials, the ion beam modification needs to be explored further.

The studies included in this thesis provide new information on precise modification of graphene via ion irradiation. The studied systems include freestanding graphene as well as metal supported graphene, with a wide range of irradiation parameters with varying ion species and energies. The presented results aim to indicate the right irradiation parameters for a specific type of lattice defects, or on the other hand, predict the damage during the irradiation. Molecular dynamics simulations are applied to study doping of freestanding graphene with boron and nitrogen, point defect production, sputtering yield under continuous irradiation, and the substrates effects on the defect production.

The results show that boron and nitrogen can be incorporated into the graphene lattice to replace exactly one carbon atom or as adatoms as has been shown earlier for carbon nanotubes [74]. The highest probability for a substitution (55%) was observed for nitrogen at about 50 eV. The low energy ensured efficient momentum transfer, therefore the ion could detach one carbon atom from the lattice and slip into its place. For different types of defects the optimal energy range varied, revealing that by changing the ion energy, one can predict which type of defect is the most probable. Estimates for sputtering yields reveals the durability of the material, showing that graphene can withstand vacancy concentrations at least up to 35%. This sets graphene as a possible candidate for window material in conditions where it has to withstand continuous irradiation.

For large scale manufacturing graphene is often grown on a substrate. The simulation results show that the substrate affects the defect production. When compared to calculations for freestanding membrane, at low energies below 1 keV, the substrate decreases the number of defects, while at higher energies it increases the probability and the complexity of them. After irradiation some of the sputtered carbon atoms are stuck at the interface between the metal surface and the graphene membrane. The free space left between the membrane and the substrate surface acts as a trap, collecting the carbon atoms that are detached from the membrane in the direction of the substrate. In the experiments, after annealing these adatoms form small graphene platelets on the metal surface. A new quantity called the trapping yield is established to describe the number of the trapped atoms per impact ion. The yields calculated from the simulations correspond to the experimentally observed sizes of the small graphene platelets. Hence, the substrate provides a way to obtain new nanostructures. On the other hand, in order to avoid these, one should apply light He^+ ions, which result in low trapping yield.

With very high energies in the MeV range, irradiation can produce hole-type defects in graphene due to inelastic scattering of the projectile from the target's electrons. The diameter of the defects can be controlled with the stopping power of the ion. The early results presented in this thesis regarding swift heavy ion irradiation of graphene already show promising results. In the near future we hope to improve the model to reproduce more accurately the unique electronic features of this material.

Although the results presented in this thesis contribute to our understanding of the behavior of two-dimensional materials under ion irradiation, the story is still unfinished. Some of the results already have experimental verification, but others lack of the comparison. The applications might require further study on specific type of irradiation parameters depending on the requirements set by the experimental setup available. Altogether, this thesis provides detailed information on the controlled modification of graphene needed when the material is to be employed in practical applications. The results can be used to indicate the right energy ranges and ion species in order to produce the desired modification. On the other hand, the calculated sputtering yields shed light on the produced damage when the material is under continuous irradiation, and the trapping yields provide information on the metal supported system. Some of the presented results have already been successfully used in experiments [76] which encourages us to continue with the work.

Acknowledgements

I wish to thank Prof. Juhani Keinonen and Prof. Hannu Koskinen, the former and the current head of the Department of Physics at the University of Helsinki, and Prof. Jyrki Räisänen, the head of the Division of Material Physics, for providing the facilities to carry out the research presented in this thesis. Financial support from University Helsinki Funds and Finnish Academy of Science and Letters are gratefully acknowledged.

My greatest gratitude goes to my tireless supervisor Docent Jani Kotakoski. His enthusiasm and energy has pushed me forward since the day one. By encouraging to independent thinking and believing in me he has been the best support a rookie scientist could hope for. Thank you for your guidance and friendship.

I would like to thank Professor Kai Nordlund, Docent Arkady Krasheninnikov and Dr. Ossi Lehtinen. With their inspiring attitude and guidance I entered the world of scientists, those mystical creatures students so often fear and respect. You inspire me as scientists as well as persons.

I thank the *Acclab* group for providing the great atmosphere. Special thanks to my office-mates for great conversations, company and cookies, for looking after me and offering help regardless of what the matter was. The *Naiset 07* for memorable study times and support. It has been an unforgettable journey.

Helsinki, 7th November 2014
Harriet

Bibliography

1. P. R. Wallace, "The Band Theory of Graphite," *Phys. Rev.*, vol. 71, pp. 622–634, 1947.

2. K. S. Novoselov, A. K. Geim, S. V. Morozov, D. Jiang, Y. Zhang, S. V. Dubonos, I. V. Grigorieva, and A. A. Firsov, "Electric Field Effect in Atomically Thin Carbon Films," *Science*, vol. 306, pp. 666–669, 2004.

3. M. Dvorak, W. Oswald, and Z. Wu, "Bandgap Opening by Patterning graphene," *Scient. Reports*, vol. 3, p. 2289, 2013.

4. J. D. Bernal, "The Structure of Graphite," *Proc. R. Soc. Lond. A*, vol. 106, pp. 749–773, 1924.

5. S. Iijama, "Helical microtubulus of graphitic carbon," *Nature*, vol. 354, pp. 56–58, 1991.

6. H. W. Kroto, J. R. Heath, S. C. O'Brien, R. F. Curl, and R. E. Smalley, "C_{60}: Buckminsterfullerene," *Nature*, vol. 318, pp. 162–163, 1985.

7. A. K. Geim and K. S. Novoselov, "The rise of graphene," *Nature Mat.*, vol. 6, p. 183, 2007.

8. R. Saito, M. Fujita, G. Dresselhaus, and M. S. Dresselhaus, "Electronic structure of graphene tubules based on C 60," *Phys. Rev. B*, vol. 46, p. 1804, 1992.

9. J. C. Slonczewski and P. R. Weiss, "Band Structure of Graphite," *Phys. Rev.*, vol. 109, pp. 272–279, 1958.

10. J. W. McClure, "Diamagnetism of Graphite," *Phys. Rev.*, vol. 104, pp. 666–671, 1956.

11. G. W. Semenoff, "Condensed-Matter Simulation of a Three-Dimensional Anomaly," *Phys. Rev. Lett.*, vol. 53, pp. 2449–2452, 1984.

12. F. D. M. Haldane, "Model for a Quantum Hall Effect without Landau Levels: Condensed-Matter Realization of the "Parity Anomaly"," *Phys. Rev. Lett.*, vol. 61, pp. 2015–2018, 1988.

13. K. Nakada, M. Fujita, G. Dresselhaus, and M. S. Dresselhaus, "Edge state in graphene ribbons: Nanometer size effect and edge shape dependence," *Phys. Rev. B.*, vol. 54, pp. 17954–17961, 1996.

14. K. Wakabayashi, M. Fujita, H. Ajiki, and M. Sigrist, "Electronic and magnetic properties of nanographite ribbons," *Phys. Rev. B.*, vol. 59, pp. 8271–8283, 1998.

15. W. A. de Heer, C. Berger, X. Wu, P. N. First, E. H. Conrad, X. Li, T. Li, M. Sprinkle, J. Hass, M. L. Sadowski, M. Potemski, and G. Martinez, "Epitaxial graphene," *Solid State Comm.*, vol. 143, pp. 92–100, 2007.

16. Y. Y. Wang, R. X. Gao, Z. H. Ni, H. He, S. P. Guo, H. P. Yang, C. X. Cong, and T. Yu, "Thickness identification of two-dimensional materials by optical imaging," *Nanotech.*, vol. 23, p. 495713, 2012.

17. S. Pei and H.-M. Cheng, "The reduction of graphene oxide," *Carbon*, vol. 50, pp. 3210–3228, 2012.

18. A. E. Karu and M. Beer, "Pyrolytic Formation of Highly Crystalline Graphite Films," *J. Appl. Phys.*, vol. 37, p. 2179, 1966.

19. C. Oshima and A. Nagashima, "Ultra-thin epitaxial films of graphite and hexagonal boron nitride on solid surfaces ," *J. Phys.: Condens. Matter*, vol. 9, p. 1, 1997.

20. X. Li, W. Cai, J. An, S. Kim, J. Nah, D. Yang, R. Piner, A. Velamakanni, I. Jung, E. Tutuc, S. K. Banerjee, L. Colombo, and R. S. Ruoff, "Large-Area Synthesis of High-Quality and Uniform Graphene Films on Copper Foils," *Science*, vol. 324, pp. 1312–1314, 2009.

21. A. Reina, X. Jia, J. Ho, D. Nezich, H. Son, V. Bulovic, M. S. Dresselhaus, and J. Kong, "Large Area, Few-Layer Graphene Films on Arbitrary Substrates by Chemical Vapor Deposition," *Nano Lett.*, vol. 9, p. 30, 2009.

22. M. Eizenberg and J. M. Blakely, "Carbon monolayer phase condensation on Ni(111)," *Surf. Sci*, vol. 82, pp. 228–236, 1979.

23. C. Lee, X. Wei, J. W. Kysar, and J. Hone, "Measurement of the Elastic Properties and Intrinsic Strength of Monolayer Graphene," *Science*, vol. 321, pp. 385–388, 2008.

24. X. Wei, B. Fragneaud, C. A. Marianetti, and J. W. Kysar, "Nonlinear elastic behavior of graphene: *Ab initio* calculations to continuum description," *Phys. Rev. B*, vol. 80, p. 205407, 2009.

25. P. Y. Huang, C. S. Ruiz-Vargas, A. M. van der Zande, W. S. Whitney, M. P. Levendorf, J. W. Kevek, S. Garg, J. S. Alden, C. J. Hustedt, Y. Zhu, J. Park, P. L. McEuen, and D. A. Muller, "Grains and grain boundaries in single-layer graphene atomic patchwork quilts," *Nature*, vol. 469, pp. 389–392, 2011.

26. C. S. Ruiz-Vargas, H. L. Zhuang, P. Y. Huang, A. M. van der Zande, S. Garg, P. L. McEuen, D. A. Muller, R. G. Hennig, and J. Park, "Softened Elastic Response and Unzipping in Chemical Vapor Deposition Graphene Membranes," *Nano Lett.*, vol. 11, pp. 2259–2263, 2011.

27. J. Kotakoski and J. C. Meyer, "Mechanical properties of polycrystalline graphene based on a realistic atomistic model," *Phys. Rev. B*, vol. 85, p. 195447, 2012.

28. N. Savvides and T. J. Bell, "Microhardness and Young's modulus of diamond and diamondlike carbon films," *J. Appl. Phys.*, vol. 72, p. 2791, 1992.

29. D. Roundy and M. L. Cohen, "Ideal strength of diamond, Si, and Ge," *Phys. Rev. B.*, vol. 64, p. 212103, 2001.

30. P. Trucano and R. Chen, "Structure of Graphite by neutron diffraction," *Nature*, vol. 258, pp. 136–137, 1975.

31. S. Reich, J. Maultzsch, and C. Thomsen, "Tight-binding description of graphene," *Phys. Rev. B.*, vol. 66, p. 035412, 2002.

32. M. Grundmann, ed., *The Physics of Semiconductors*. Berlin Heidelberg: Springer-Verlag, 2010.

33. K. S. Novoselov, S. V. Morozov, T. M. G. Mohinddin, L. A. Ponomarenko, D. C. Elias, R. Yang, I. Barbolina, P. Blake, T. J. Booth, D. Jiang, J. Giesbers, E. W. Hill, and A. K. Geim, "Electronic properties of graphene," *Phys. Stat. Sol. B*, vol. 244, pp. 4106–4111, 2007.

34. A. H. C. Neto, F. Guinea, N. M. R. Peres, K. S. Novoselov, and A. K. Geim, "The electronic properties of graphene," *Rev. of Modern Phys.*, vol. 81, pp. 109–162, 2009.

35. Y. Zheng and T. Ando, "Hall conductivity of a two-dimensional graphite system," *Phys. Rev. B*, vol. 65, p. 245420, 2002.

36. L. Ci, L. Song, C. Jin, D. Jariwala, D. Wu, Y. Li, A. Srivastava, Z. F. Wang, K. Storr, L. Balicas, F. Liu, and P. Ajayan, "Atomic layers of hybridized boron nitride and graphene domains," *Nature Mat.*, vol. 9, pp. 430–435, 2010.

37. W. H. Brito, R. Kagimura, and R. H. Miwa, "B and N doping in graphene ruled by grain boundary defects," *Phys. Rev. B*, vol. 85, p. 035404, 2012.

38. B. Guo, Q. Liu, E. Chen, H. Zhu, L. Fang, and J. R. Gong, "Controllable N-doping of graphene," *Nano Lett.*, vol. 10, pp. 4975–4980, 2010.

39. L. S. Panchokarla, K. S. Subrahmanyam, S. K. Saha, A. Govindaraj, H. R. Krishnamurthy, U. V. Waghmare, and C. N. R. Rao, "Synthesis, Structure, and Properties of Boron- and Nitrogen-Doped Graphene," *Adv. Mat.*, vol. 21, pp. 4726–4730, 2009.

40. T. C. M. Chung, Y. Jeong, Q. Chen, A. Kleinhammes, and Y. Wu, "Synthesis of Microporous Boron-Substituted Carbon (B/C) Materials Using Polymeric Precursors of Hydrogen Physisorption," *J. Am. Chem. Soc.*, vol. 130, p. 6668, 2008.

41. R. B. Pontes, A. Fazzio, and G. M. Dalplan, "Barrier-free substitutional doping of graphene sheets with boron atoms: *Ab initio* calculations," *Phys. Rev. B*, vol. 79, p. 033412, 2009.

42. T. O. Wehling, K. S. Novoselov, S. V. Morozov, E. E. Vdovin, M. I. Katsnelson, A. K. Geim, and A. I. Lichtenstein, "Molecular doping of Graphene," *Nano Lett.*, vol. 8, pp. 173–177, 2008.

43. B. Wang and S. T. Pantelides, "Controllable healing of defects and nitrogen doping of graphene by CO and NO molecules," *Phys. Rev. B*, vol. 83, p. 245403, 2011.

44. A. Zandiatashbar, G.-H. Lee, S. J. An, S. Lee, N. Mathew, M. Terrones, T. Hayashi, C. R. Picu, J. Hone, and N. Koratkar, "Effect of defects on the intrinsic strenght and stiffness of graphene," *Nature Comm.*, vol. 5, p. 3186, 2014.

45. D. Kanjijal, "Swift heavy ion-induced modification and track formation in materials," *Current Science*, vol. 80, no. 12, p. 1560, 2001.

46. A. A. Leino, S. L. Daraszewicz, O. H. Pakarinen, F. Djurabekova, K. Nordlund, B. Afra, and P. Kluth, "Structural analysis of simulated swift heavy ion tracks in quartz," *Nucl. Instr. Meth. Phys. Res. B*, vol. 326, pp. 289–292, 2014.

47. R. L. Fleischer, P. B. Price, and R. M. Walker, "Ion explosion Spike Mechanism for Formation of Charged-Particle Tracks in Solids," *J. Appl. Phys.*, vol. 36, p. 3645, 1965.

48. G. Szenes, "Comparison of two thermal spike models for ion-solid interaction," *Nucl. Instr. Meth. Phys. Res. B*, vol. 269, pp. 174–179, 2011.

49. K. H. Bennemann, "Ultrafast dynamics in solids," *J. Phys.: Condens. Matter*, vol. 16, pp. R995–R1056, 2004.

50. S. Akcöltekin, H. Bukowska, T. Peters, O. Osmani, I. Monnet, I. Alzaher, B. B. d'Etat, H. Lebius, and M. Schleberger, "Unzipping and folding of graphene by swift heavy ions," *Appl. Phys. Lett.*, vol. 98, p. 103103, 2011.

51. O. Ochedowski, S. Akcöltekin, B. Ban-d'Etat, H. Lebius, and M. Schleberger, "Detecting swift heavy ion irradiation effects with graphene," *Nucl. Inst. and Meth. in Phys. Res. B*, vol. 314, pp. 18–20, 2013.

52. M. Born and R. Oppenheimer, "Zur Quantentheorie der Molekeln," *Ann. Phys.*, vol. 389, p. 457, 1927.

53. K. Nordlund, "Molecular dynamics simulation of ion ranges in the 1–100 keV energy range," *Comp. Mat. Sci.*, vol. 3, p. 448, 1995.

54. B. J. Alder and T. E. Wainwright, "Phase Transitions for a Hard Sphere System," *J. Chem. Phys.*, vol. 27, p. 1208, 1957.

55. B. J. Alder and T. E. Wainwright, "Studies in Molecular Dynamics I. General Method," *J. Chem. Phys.*, vol. 31, p. 459, 1959.

56. B. J. Alder and T. E. Wainwright, "Studies in Molecular Dynamics II. Behavior of a Small Number of Elastic Spheres," *J. Chem. Phys.*, vol. 33, p. 1439, 1960.

57. M. P. Allen and D. J. Tildesley, eds., *Computer Simulation of Liquid*. England: Oxford University Press, 1987.

58. M. P. R. Waligorski, R. N. Hamm, and R. Katz, "The radial distribution of dose around the path of a heavy ion in liquid water," *Nucl. Track. Radiat. Meas.*, vol. 11, pp. 309–319, 1986.

59. D. S. Ivanov and L. V. Zhigilei, "Combined atomistic-continuum modeling of short-pulse laser melting and disintegration of metal films," *Phys. Rev. B*, vol. 68, pp. 064114–22, 2003.

60. E. Schrödinger, "An Undulatory Theory of the Mechanics of Atoms and Molecules," *Phys. Rev.*, vol. 28, pp. 1049–1070, 1926.

61. P. Hohenberg and W. Kohn, "Inhomogenous Electron Gas," *Phys. Rev. B*, vol. 136, p. B867, 1964.

62. W. Kohn and L. J. Sham, "Self-Consistent Equations Including Exhange and Correlation Effects," *Phys. Rev.*, vol. 140, p. A1133, 1965.

63. P. M. Morse, "Diatomic Molecules According to the Wave Mechanics II. Vibrational Levels," *Phys. Rev.*, vol. 34, p. 57, 1929.

64. J. Tersoff, "Empirical Interatomic Potential for Carbon, with Applications to Amorphous Carbon," *Phys. Rev. Lett.*, vol. 61, pp. 2879–2882, 1988.

65. J. Tersoff, "New empirical approach for the structure and energy of covalent systems," *Phys. Rev. B*, vol. 37, pp. 6991–7000, 1988.

66. D. W. Brenner, O. A. Shenderova, J. A. Harrison, S. J. Stuart, B. Ni, and S. B. Sinnott, "A second-generation reactive empirical bond order (REBO) potential energy expression for hydrocarbons," *J. Phys.: Condens. Matter*, vol. 14, pp. 783–802, 2002.

67. D. W. Brenner, "Empirical potential for hydrocarbons for use in simulating the chemical vapor deposition of diamond films," *Phys. Rev. B*, vol. 42, pp. 9458–9471, 1990.

68. K. Matsunaga, C. Fisher, and H. Matsubara, "Potential Parameters for Simulating Cubic Boron Carbonitrides ," *Jpn. J. Appl. Phys.*, vol. 39, pp. L48–L51, 2000.

69. J. F. Ziegler, J. P. Biersack, and U. Littmark, eds., *The Stopping and Range of Ions in Matter*. New York: Pergamon, 1985.

70. K. Nordlund, N. Runeberg, and D. Sundholm, "Repulsive interatomic potentials calculated using Hartree-Fock and density-functional theory methods," *Nucl. Instrum. Methods Phys. Res. B*, vol. 123, p. 45, 1997.

71. H. J. C. Berendsen, J. P. M. Postma, W. F. van Gunsteren, A. DiNola, and J. R. Haak, "Molecular dynamics with coupling to an external bath," *J. Chem. Phys.*, vol. 81, p. 3684, 1984.

72. G. Binnig, H. Rohrer, C. Gerber, and E. Weibel, "Tunneling through a controllabe gap," *Appl. Phys. Lett.*, vol. 40, p. 178, 1982.

73. O. Lehtinen, J. Kotakoski, A. V. Krasheninnikov, A. Tolvanen, K. Nordlund, and J. Keinonen, "Effects of ion bombardment on a two-dimensional target: Atomistic simulations of graphene irradiation," *Phys. Rev. B*, vol. 81, p. 153401, 2010.

74. J. Kotakoski, A. V. Krasheninnikov, Y. Ma, A. S. Foster, K. Nordlund, and R. M. Nieminen, "B and N ion implantation into carbon nanotubes: Insight from atomistic simulations," *Phys. Rev. B*, vol. 71, p. 205408, 2005.

75. P. O. Lehtinen, A. S. Foster, A. Ayuela, A. V. Krasheninnikov, K. Nordlund, and R. M. Nieminen, "Magnetic Properties and Diffusion of Adatoms on a Graphene Sheet," *Phys. Rev. Lett.*, vol. 91, p. 017202, 2003.

76. U.Bangert, W. Pierce, D. M. Kepaptsoglou, Q. Ramasse, R. Zan, M. H. Gass, J. A. V. den Berg, C. B. Boothroyd, J. Amani, and H. Hohsäss, "Ion Implantation of Graphene - Toward IC Compatible Technologies," *Nano Lett.*, vol. 13, pp. 4902–4907, 2013.

77. E. Stolyarova, D. Stolyarov, K. Bolotin, S. Ryu, L. Liu, K. T. Rim, M. Klima, M. Hybertsen, I. Pogorelsky, I. Pavlishin, K. Kusche, J. Hone, P. Kim, H. L. Stormer, V. Yakimenko, and G. Flynn, "Observation of Graphene Bubbles and Effective Mass Transport under Graphene Films," *Nano Lett.*, vol. 9, pp. 332–337, 2009.

78. J. S. Bunch, S. S. Verbridge, J. S. Aldena, A. M. van der Zande, J. M. Parpia, H. G. Craighead, and P. L. McEuen, "Impermeable Atomic Membranes from Graphene Sheets," *Nano Lett.*, vol. 8, pp. 2458–2462, 2008.

79. O. Leenaerts, B. Partoens, and F. M. Peeters, "Graphene: A perfect nanoballoon," *Appl. Phys. Lett.*, vol. 93, p. 193107, 2008.

80. M. Gao, Y. Pan, C. Zhang, H. Hu, R. Yang, H. Lu, J. Cai, S. Du, F. Liu, and H.-J. Gao, "Tunable interfacial propeties of epitaxial graphene on metal substrates," *Appl. Phys. Lett.*, vol. 96, p. 053109, 2010.

81. P. Sutter, J. T. Sadowski, and E. Sutter, "Graphene on Pt(111): Growth and substrate interaction," *Phys. Rev. B*, vol. 80, p. 245411, 2009.

82. G. Otero, C. Gonzalez, A. L. Pinardi, P. Merino, S. Gardonio, S. Lizzit, M. Blanco-Rey, K. V. de Ruit, C. F. J. Flipse, J. Mendez, P. L. de Andres, and J. A. Martin-Gago, "Ordered Vacancy Network Induced by the Growth of Epitaxial Graphene on Pt(111)," *Phys. Rev. Lett*, vol. 105, p. 216102, 2010.

83. S. Standop, O. Lehtinen, C. Herbig, G. Lewes-Malandrakis, F. Craes, J. Kotakoski, T. Michely, A. V. Krasheninnikov, and C. Busse, "Ion Imapacts on Graphene/Ir(111): Interface Channeling, Vacancy Funnels, and a Nanomesh," *Nano Lett.*, vol. 13, pp. 1948–1955, 2013.

84. J. C. Johannsen, S. Ulstrup, F. Cilento, A. Crepaldi, M. Zacchigna, C. Cacho, I. C. E. Turcu, E. Springate, F. Fromm, C. Raidel, T. Seyller, F. Parmigiani, M. Grioni, and P. Hofmann, "Direct View of Hot Carrier Dynamics in Graphene," *Phys. Rev. Lett.*, vol. 111, p. 027403, 2013.

85. V. S. Katti and S. S. Kubakaddi, "Electronic thermal conductivity in suspended and supported bilayer graphene," *Physica E: Low-dimens. Sys. and Nanostr.*, vol. 47, pp. 188–192, 2013.

86. S. Yigen, V. Tayari, J. O. Island, J. M. Porter, and A. R. Champagne, "Electronic thermal conductivity measurements in intrinsic graphene," *Phys. Rev. B*, vol. 87, p. 241411, 2013.

87. Private communication with Oliver Ochedowski, 10.08.2014.

88. G. F. Schneider, S. W. Kowalczyk, V. E. Calado, G. Pandraud, H. W. Zandbergen, L. M. K.Vandersypen, and C. Dekker, "DNA Translocation through Graphene Nanopores," *Nano Lett.*, vol. 10, pp. 3163–3167, 2010.

89. D. Jiang, V. R. Cooper, and S. Dai, "Porous Graphene as the Ultimate Membrane for Gas Separation," *Nano Lett.*, vol. 9, pp. 4019–4024, 2009.

90. J. Schrier, “Helium Separation Using Porous Graphene Membranes,” *J. Phys. Chem. Lett.*, vol. 1, pp. 2284–2287, 2010.

91. S. Koenig, L. Wang, J. Pellegrino, and J. S. Bunch, “Selective molecular sieving through porous graphene,” *Nature Nanotech.*, vol. 7, pp. 728–732, 2012.

92. D. Cohen-Tanugi and J. C. Grossman, “Water Desalination across Nanoporous Graphene,” *Nano Lett.*, vol. 12, pp. 3602–3608, 2012.